Vehicle Dynamics Control for Rollover Prevention

Schofield, Brad

2006

Document Version:
Publisher's PDF, also known as Version of record

Vehicle Dynamics Control for Rollover Prevention

Brad Schofield

Department of Automatic Control
Lund University
Lund, December 2006

Department of Automatic Control
Lund University
Box 118
SE-221 00 LUND
Sweden

ISSN 0280–5316
ISRN LUTFD2/TFRT--3241--SE

Printed in Sweden,
Lund University, Lund 2006

Acknowledgments

First of all I would like to thank everyone at the department for helping to create such an attractive working environment, which I have had the privilege of sharing for the past three years. I would particularly like to thank my supervisors Tore Hägglund and Anders Rantzer for their guidance, support and advice.

Special thanks go to Dr. Jens Kalkkuhl at DaimlerChrysler for his hard work in coordinating the project and his invaluable insight into the complex world of vehicle dynamics.

A number of people at the department deserve special mention, not least my former roommate Ather Gattami, who consistently kept the whiteboard covered with rather intimidating mathematics. The unenviable task of proofreading this thesis was undertaken by Martin Ansbjerg Kjær, for which I am grateful. Thanks also go to Leif Andersson, for answering all of my computing-related questions, of which there have been many. I would also like to thank Anders Robertsson, for always finding the time to answer my (often rather obscure) questions, as well as Eva Schildt, Britt-Marie Mårtensson and Agneta Tuszynski, who ensure the smooth running of the department.

The work was funded by the EU 6th framework project *Complex Embedded Automotive Control Systems* (CEmACS).

I would particularly like to mention those current and former members of the department with whom I have participated in a range of non-control-related activities, such as hiking, climbing, cycling, skiing, music and beer-drinking. These include Oskar Nilsson, Stéphane Velut, Staffan Haugwitz and Johan Bengtsson, to name but a few.

Finally I would like to thank my parents, for their continued encouragement and support, despite my disappearance to a different country for the duration of my Ph.D. The final word here goes to my brother, the only person I know who shares my definition of freezing conditions, heavy packs, blistered feet and exhaustion as a 'holiday'.

Contents

1. Introduction 7
- 1.1 Background 7
- 1.2 Motivation 8
- 1.3 Scope 9
- 1.4 Outline 10
- 1.5 Publications 10

2. Vehicle Modeling 11
- 2.1 Introduction 11
- 2.2 Tire models 11
- 2.3 Chassis Models 16

3. Rollover Analysis and Detection 34
- 3.1 Introduction 34
- 3.2 Static Rollover Analysis 34
- 3.3 Stability 37
- 3.4 Load Transfer 39
- 3.5 Methods for Rollover Detection 42

4. Controller Design 48
- 4.1 Introduction 48
- 4.2 Control Strategy 50
- 4.3 Roll Control 52
- 4.4 Yaw Control 54
- 4.5 Summary 60

5. Control Allocation 61

5.1 Introduction 61
5.2 Problem Formulation 61
5.3 Convex Optimization 62
5.4 Solving Convex Optimization Problems 64
5.5 Control Allocator Design 65
6. Results 78
6.1 Introduction 78
6.2 Test Maneuvers 79
6.3 Simulation Results 81
6.4 Discussion 100
7. Conclusions and Future Work 103
7.1 Summary 103
7.2 Conclusions 104
7.3 Future Work 104
8. Bibliography 106

1

Introduction

1.1 Background

Many of the recent advances in automotive technology are based on control. Engine control is widely used as a means of increasing performance and efficiency while reducing emissions, to the extend that new engine types are being developed which cannot operate without a feedback control system [Bengtsson, 2004; Kiencke and Nielsen, 2000]. Active safety is another area of automotive engineering dominated by control technology. Anti-lock braking systems were introduced in the 1970's as a means of reducing braking distances, and modern versions use advanced control algorithms. Traction control systems can use the ABS system as an actuator, the functionality being provided by a controller. More recently, higher-level active safety systems have come into production, such as Electronic Stability Programs (ESP) which prevent skidding. Such systems, which govern the stability of the entire vehicle rather than just certain components, may be grouped under the heading of Vehicle Dynamics Control (VDC) systems. This thesis deals with a new kind of VDC system, capable of preventing vehicle rollover accidents.

There are are number of difficulties associated with automotive control, which can transform even apparently simple control tasks into considerable challenges. These difficulties include:

- **Uncertainty**. There is a large number of parameters, states and

other variables, used by the controller, which either cannot be measured or are not known exactly. Examples include the loading conditions, particularly in the case of commercial vehicles, and the coefficient of friction between the tire and the road surface. For cost reasons, sensors are typically kept to a minimum in production vehicles and as such it is often necessary to estimate variables, which gives rise to additional uncertainty.

- **Complexity**. Vehicles are complex systems, with many degrees of freedom. Control systems are often multivariable, with many actuators and output signals. The equations governing the behaviour of the system are very often highly nonlinear, meaning that standard linear control design tools may not always be applicable.
- **Reliability and Robustness**. For production vehicles it is imperative that system operation can be guaranteed for a wide range of operating conditions. The high level of robustness required may mean that performance requirements are difficult to meet.

Currently, vehicles contain a number of different control systems which deal with different aspects of vehicle operation. As the number of control systems within a vehicle grows, so too does the interaction between the systems. If the systems are designed independently, it is likely that unwanted interactions between different systems will give rise to degraded performance. A current trend is to integrate the control systems within the vehicle. One aspect of this integration is the development of unified vehicle dynamics control systems. Although the focus of this thesis is rollover prevention, the couplings present in the dynamics of the vehicle imply that this problem cannot be studied in isolation, but must be viewed in a wider context of vehicle dynamics control.

1.2 Motivation

Vehicle rollover accidents may be grouped into two categories, known as *tripped* and *untripped* rollovers respectively. Tripped rollovers are

caused by the vehicle coming into contact with an external obstacle, such as a curb or a pothole. This type of rollover accident may sometimes be avoided by the use of ESP systems, which prevent oversteering and understeering, thus preventing collisions with external obstacles.

Untripped rollovers are induced by extreme driving maneuvers, in which the forces at the tire-road contact point are sufficient to cause the vehicle to roll over.

Vehicle rollover accidents are typically very dangerous. Research by the National Highway Traffic Safety Administration (NHTSA) in the United States shows that rollover accidents are the second most dangerous form of accident in the Unites States, after head-on collisions. In 2000, 9,882 people were killed in the US in rollover accidents involving light vehicles [Forkenbrock *et al.*, 2002]. 8,146 of those were killed in accidents involving only a single vehicle. While the majority of these accidents involved tripped rollovers, it is clear that an active safety system capable of preventing untripped rollover accidents will save lives, and as such is worthy of investigation. Moreover, the expansion of functionality of active safety systems is in keeping with the trend towards greater integration of control design in automotive vehicles.

1.3 Scope

The design of a complete vehicle dynamics control system involves many aspects of control engineering, including the selection of actuators, design of parameter estimation schemes and state observers, as well as the control design itself. This thesis concentrates on the control design aspects. It is assumed that estimates of the vehicle states are available to the control algorithm. In addition, the necessary vehicle parameters, including the loading conditions, are assumed to be known. This is of course unrealistic for a production system, and the removal of this assumption constitutes a major direction for future research on the subject.

There is also considerable freedom in the choice of actuators to be used. Active steering, differential braking and active suspension, as well as combinations thereof may be considered. Active suspension is the most hardware-demanding actuator choice. Active steering and braking are often used together in rollover prevention systems [Oden-

thal *et al.*, 1999]. However, active steering requires additional hardware, in the form of either a mechanical superposition actuator or a full steer-by-wire system. Differential braking, achieved by using a braking system with Electronic Brake force Distribution (EBD), is already in use in various production vehicles, and as such represents the most realistic actuator choice. This thesis uses differential braking as the actuator, although it will be seen that the methods developed may be easily extended to other types of actuators, as well as combinations of different actuators. The types of vehicle primarily considered in this work are small commercial vehicles such as vans and trucks. However, the ideas presented may be easily applied to other types of vehicle, such as larger trucks.

1.4 Outline

The thesis begins with a chapter dedicated to vehicle modeling. Both tyre models and chassis models are presented. A number of models of varying levels of complexity are derived. Different models are required for different purposes, such as control design, reference generation and simulation. Chapter 3 deals with analysis of the rollover problem, beginning with simple static analysis, as well as methods for detection of rollover events. In Chapter 4 the design methodology is presented, and control design is carried out. The concept of *Control Allocation*, on which the control strategy is based, is presented in Chapter 5. Finally, results are presented and discussed in Chapter 6.

1.5 Publications

Elements of the control design presented in Chapter 4, as well as the control allocation strategy presented in Chapter 5 are based on the following paper:

Schofield, B., T. Hägglund and A. Rantzer (2006): "Vehicle Dynamics Control and Controller Allocation for Rollover Prevention." In *Proceedings of the IEEE International Conference on Control Applications*, Munich, Germany.

2

Vehicle Modeling

–It's only a model!
Terry Gilliam (Monty Python)

2.1 Introduction

Most modern control design methodologies are model-based. The first step in the design process therefore consists of obtaining a suitable model. In many cases several models are required for different purposes, such as design, reference generation, and simulation. In this chapter some standard approaches to vehicle modeling are introduced, and a number of models are derived.

Vehicle modeling is divided into two areas: tire modeling and chassis modeling. Tire modeling deals with understanding the forces that arise at the tire-road contact point. Chassis modeling involves determining the behaviour of the vehicle when subject to these external forces. The chapter begins with a brief introduction to tire modeling, in which some simple models are described. Chassis modeling is then performed yielding a number of models of different complexities.

2.2 Tire models

All road vehicles interact with the road surface via tires. More specifically, the tires are responsible for generating those forces which are

required to alter the vehicle's speed and course according the driver's inputs.

The physical mechanisms by which tires function are complicated, and modelling is therefore difficult. A variety of different models exists, both theoretical and empirical. In this section a widely-used approach to tire modeling will be presented.

Slip

In order to generate forces, the tires must *slip*. Slip occurs in different planes of the tire's motion. Longitudinal slip will be considered first. When the tire is rolling freely (no driving or braking force applied),

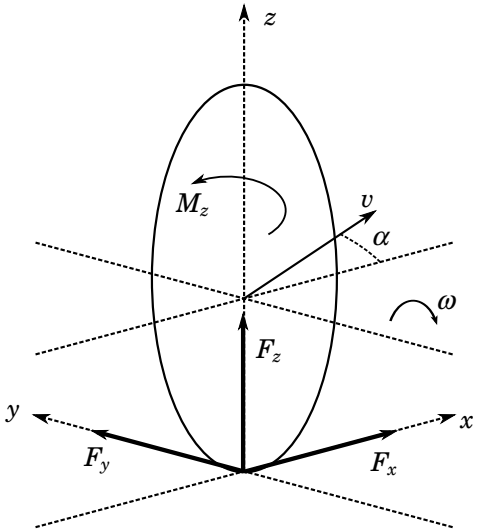

Figure 2.1 Diagram of a wheel showing its local axes, the components of the forces acting at the road contact point, the angular velocity ω and the translational velocity v. The x axis corresponds to the direction of travel of the wheel when no sideslip occurs.

the *effective rolling radius* r_e may be defined as follows:

$$r_e = \frac{v_x}{\omega_0}$$

where v_x is the component of the velocity v in the x direction, and ω_0 is the wheel's angular velocity. Figure 2.1 illustrates the coordinate system of the wheel. When a driving or braking torque is applied to the wheel, longitudinal slip develops:

$$\begin{aligned}\lambda &= -\frac{v_x - r_e\omega}{v_x} \\ &= -\frac{\omega_0 - \omega}{\omega_0}\end{aligned}$$

where ω is the measured angular velocity of the wheel. The longitudinal slip λ is defined in such a way that a positive (driving) force gives a positive slip value. With the above definition, slip values can be much larger than one (in the case of wheel spin). It is possible to define slip in an alternative way, with ω in the denominator, which would give a maximum slip value of one.

The lateral slip is the ratio of the wheel's velocities in the y and x directions. It can be defined through the lateral slip angle α as follows:

$$\tan\alpha = -\frac{v_y}{v_x}$$

The definition is such that positive side forces correspond to positive slip angles.

An additional slip quantity is known as spin, and is caused by rotation of the wheel about the z axis. The wheel camber angle γ, defined as the angle between the wheel's xz plane and the vertical, influences this quantity.

The Tire System

The tire may be regarded as a system having the slip components as inputs, and the forces F_x, F_y and moment M_z as outputs [Pacejka, 2002]:

$$\begin{aligned}F_x &= F_x(\lambda, \alpha, \gamma, F_z) \\ F_y &= F_y(\lambda, \alpha, \gamma, F_z) \\ M_z &= M_z(\lambda, \alpha, \gamma, F_z)\end{aligned}$$

where F_z is the wheel load. Although the z axis is directed downwards, it is standard to define the F_z forces as being positive in an upwards direction. Additionally, the camber angle γ will be assumed to be zero, reducing the dependence of the forces to three variables.

Pure and Combined Slip

Pure slip is used to denote when a given slip quantity appears in isolation, that is, when all other slip quantities are zero. To derive expressions for the tire system's outputs F_x, F_y and M_z, the pure slip case will be considered first, and then extended to combined slip.

A simple linear approximation can be made in the pure slip case by examining the gradient of the force-slip characteristic. Due to the shape of the curves, the approximations are valid only for small slip values. The approximations are given by:

$$F_x \approx C_{F_\lambda} \lambda \tag{2.1a}$$

$$F_y \approx C_{F_\alpha} \alpha \tag{2.1b}$$

$$M_z \approx -C_{M\alpha} \alpha \tag{2.1c}$$

Here, $C_{F\lambda}$ is the longitudinal slip stiffness, $C_{F\alpha}$ is the lateral slip stiffness and $C_{M\alpha}$ is known as the aligning stiffness.

A more accurate expression for the lateral force F_y is given by the so-called *Magic Formula* [Pacejka, 2002]:

$$F_y = D \sin[C \arctan\{B\alpha - E(B\alpha - \arctan(B\alpha))\}] \tag{2.2}$$

where:

$B = \dfrac{C_{F\alpha}}{CD}$ is the stiffness factor

$D = \mu F_z = F_{y,peak}$ is the peak factor

$C_{F\alpha} = c_1 \sin\left(2 \arctan\left(\dfrac{F_z}{c_2}\right)\right)$

C, E are shape factors

c_1 is the maximum cornering stiffness

c_2 is the load at maximum cornering stiffness

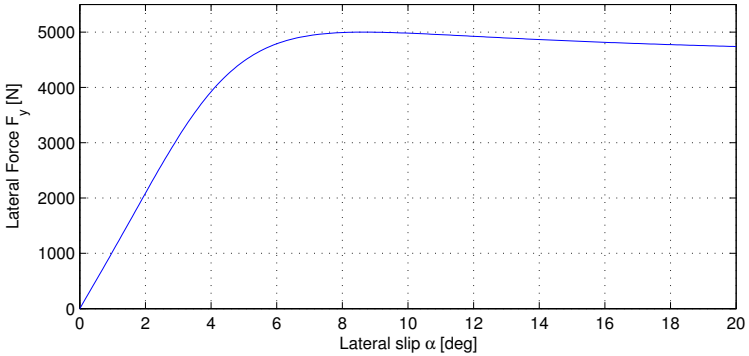

Figure 2.2 The relation between lateral force F_y and slip angle α obtained using the Magic Formula (2.2).

Figure 2.2 illustrates the relation between slip angle and lateral force, for typical parameter values.

Combined slip is the term used to describe the situation in which multiple slip types occur. Here, the case where lateral and longitudinal slips are nonzero will be considered. A common technique used for modelling this type of combined slip is based on the idea of the *friction ellipse*, shown in Figure 2.3. The assumption is that the longitudinal and lateral forces acting on each tire cannot exceed their maximum values $F_{x,max}$ and $F_{y,max}$, and the resultant force thus lies on the ellipse given by:

$$\left(\frac{F_y}{F_{y,max}}\right)^2 + \left(\frac{F_x}{F_{x,max}}\right)^2 = 1 \tag{2.3}$$

The friction ellipse idea can be confirmed empirically by plotting curves of the forces F_x and F_y for different slip values and noting that the envelope of the curves approximates an ellipse [Wong, 1993].

The maximum lateral force $F_{y,max}$ may be taken to be given by the magic formula (2.2). The maximum longitudinal force is taken to be given by the product of the coefficient of friction between the tire and

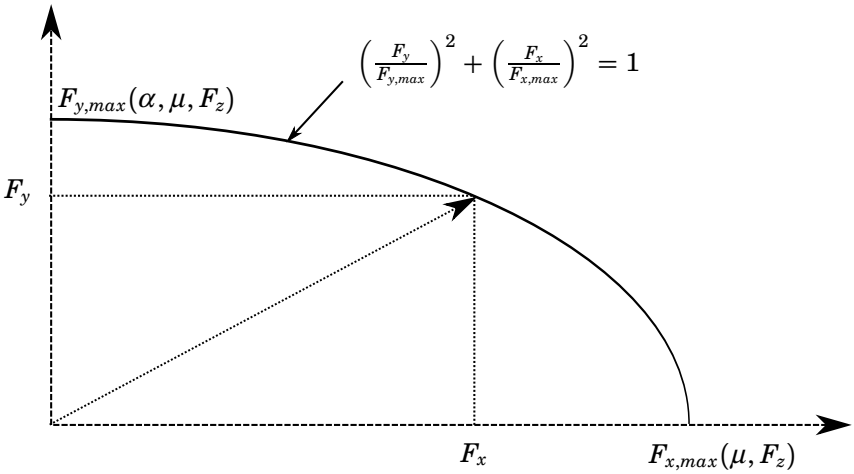

Figure 2.3 The friction ellipse, showing maximum lateral and longitudinal forces, the resultant force and its components.

the road surface (μ) and the normal force F_z acting on the tire:

$$F_{x,max} = \mu F_z$$

2.3 Chassis Models

The tire models described in the previous section are used to obtain the contact forces between the tires and the road surface. These forces constitute the inputs to the chassis model, which describes the motion of the vehicle in space. In this section, several chassis models of varying complexity will be derived. Models of different complexities are required for different applications, such as control design, reference generation and simulation. As well as these concrete applications, the process of modeling is extremely important for gaining an understanding of the system, which is vital when choosing a control strategy.

The section begins with an introduction to the coordinate systems used in the representation of the vehicle's motion. A simple linear

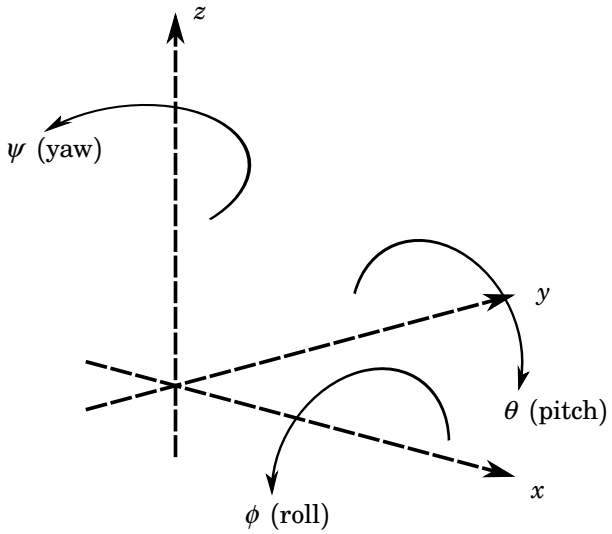

Figure 2.4 The coordinate axes. The x axis corresponds to the longitudinal axis of the vehicle, positive in the forward direction. The y axis corresponds to the lateral axis, positive to the left. Roll, pitch and yaw are defined around the x, y and z axes respectively.

model describing the planar motion of the vehicle is then introduced. This model is extended to include a description of the roll dynamics. Four degree-of-freedom models are then derived, using two modeling approaches.

Coordinate Systems

In order to facilitate the derivation of the equations of motion, it is useful to define a number of coordinate systems. This allows a more systematic approach to modeling, which is particularly important when dealing with more complex models. Figure 2.4 illustrates a right-hand coordinate system. *Roll*, *pitch* and *yaw* are defined as rotations around the x, y and z axes respectively.

Let S_i denote an earth-fixed inertial right-hand coordinate system, with the z axis oriented upwards relative to the earth. Denote with S_v a coordinate system attached to the vehicle, which rotates with angular

velocity $\omega_i^v = (0 \quad 0 \quad \dot{\psi})^T$ about the z axis, and translates in the xy plane with velocity $(u \quad v \quad 0)^T$. In addition, let S_c denote a chassis coordinate system, rotated an angle θ about the y axis of the S_v frame. The x axis of the chassis coordinate system is the roll axis, about which the roll angle ϕ is defined. Finally, denote with S_b a body coordinate system which rotates around the x axis of the chassis system with angular velocity $\omega_c^b = (\dot{\phi} \quad 0 \quad 0)^T$ The position of the centre of gravity (CG) in the body frame is given by $P_{CG}^b = (0 \quad 0 \quad h)^T$.

In the derivations of the models it will be necessary to transform between these coordinate systems. To this end, rotation matrices may be defined. The rotation matrix from the inertial system S_i to the vehicle system S_v is defined as:

$$R_i^v(\psi) = \begin{pmatrix} \cos(\psi) & -\sin(\psi) & 0 \\ \sin(\psi) & \cos(\psi) & 0 \\ 0 & 0 & 1 \end{pmatrix} \tag{2.4}$$

The rotation matrix from the vehicle system S_v to the chassis system S_c is given by:

$$R_v^c(\theta) = \begin{pmatrix} \cos(\theta) & 0 & \sin(\theta) \\ 1 & 1 & 0 \\ -\sin(\theta) & 0 & \cos(\theta) \end{pmatrix} \tag{2.5}$$

The rotation matrix from the chassis system S_c to the body system S_b is given by:

$$R_c^b(\phi) = \begin{pmatrix} 1 & 0 & 0 \\ 0 & \cos(\phi) & -\sin(\phi) \\ 0 & \sin(\phi) & \cos(\phi) \end{pmatrix} \tag{2.6}$$

A rotation from the inertial system S_i to the body system S_b can be expressed as the product of the above rotation matrices:

$$R_i^b(\psi, \theta) = R_c^b(\phi) R_v^c(\theta) R_i^v(\psi) \tag{2.7}$$

Since the rotation matrices are skew-symmetric, the relation:

$$RR^T = R^T R = I$$

may be used to obtain the rotation matrices for rotations in the opposite direction. Due to the special structure of the matrices, this may be thought of as rotation by a negative angle:

$$R_i^v(\psi) = R_v^i(-\psi)$$

When dealing with moving coordinate systems, the expressions for velocities and accelerations become more complex due to the need to express these quantities in inertial frames when they are to be used in equations of motion. Consider a point described by the vector P relative to a body-fixed frame. Assume that the origin of the body system is translated by a vector R from the origin of an inertial frame, and that the body frame rotates with angular velocity ω relative to the inertial frame. The expression for the velocity of the point P in the inertial frame is given by:

$$\left.\frac{dP}{dt}\right|_i = \frac{dR}{dt} + \left.\frac{dP}{dt}\right|_b + \omega_i^b \times P \tag{2.8}$$

Similarly, the acceleration of the point P in the inertial frame is given by:

$$\left.\frac{d^2P}{dt^2}\right|_i = \frac{d^2R}{dt^2} + \left.\frac{dP^2}{dt^2}\right|_b + \dot{\omega}_i^b \times P + 2\omega_i^b \times \left.\frac{dP}{dt}\right|_b + \omega_i^b \times (\omega_i^b \times P) \tag{2.9}$$

Linear Single-Track Model

The simplest chassis model is the linear single-track model, also known as the bicycle model, which is obtained by approximating the front and rear pairs of wheels as single wheels and linearizing the equations. The model is illustrated in Figure 2.5. Assuming that the steering angle δ is small, the equations of motion are given by [Pacejka, 2002]:

$$\begin{aligned} m(\dot{v} + u\dot{\psi}) &= F_{yF} + F_{yR} \\ I_{zz}\ddot{\psi} &= aF_{yF} - bF_{yR} \end{aligned}$$

where F_{yF} and F_{yR} are the combined front and rear lateral tire forces, I_{zz} is the moment of inertia around the z axis, a and b are the distances

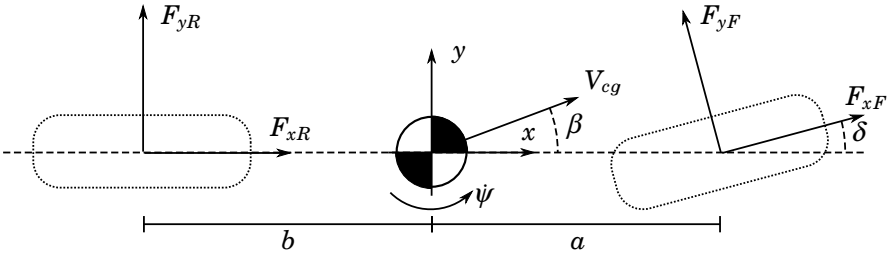

Figure 2.5 Single-track model, showing the combined front and rear tire forces, the steering angle δ, the yaw rate *psi*, and the vehicle sideslip angle β.

from the front and rear wheels to the center of gravity, and $\dot{\psi}$ is the yaw rate. The slip angles of the front and rear wheels α_F and α_R can be approximated as:

$$\alpha_F \approx \delta - \frac{1}{u}(v + a\dot{\psi}) \tag{2.10a}$$

$$\alpha_R \approx -\frac{1}{u}(v - b\dot{\psi}) \tag{2.10b}$$

Linear approximations of the tire forces, as described in (2.1a), may be used to obtain simple expressions for the tire forces:

$$F_{yF} \approx C_{F_\alpha}\alpha_F \tag{2.11a}$$

$$F_{yR} \approx C_{R_\alpha}\alpha_R \tag{2.11b}$$

The model becomes linear and time invariant if it is assumed that the forward velocity u is constant. This results in a two degree of freedom model, with the lateral velocity v and yaw rate $\dot{\psi}$ as states. The input is the steering angle δ. The system may be written on state space form as:

$$\begin{pmatrix} \dot{v} \\ \ddot{\psi} \end{pmatrix} = \begin{pmatrix} -\frac{C_{F\alpha}+C_{R\alpha}}{mu} & \frac{bC_{R\alpha}-aC_{F\alpha}}{mu} - u \\ \frac{bC_{R\alpha}-aC_{F\alpha}}{I_{zz}u} & -\frac{a^2C_{F\alpha}-b^2C_{R\alpha}}{I_{zz}u} \end{pmatrix} \begin{pmatrix} v \\ \dot{\psi} \end{pmatrix} + \begin{pmatrix} \frac{C_{F\alpha}}{m} \\ \frac{aC_{F\alpha}}{I_{zz}} \end{pmatrix} \delta \tag{2.12}$$

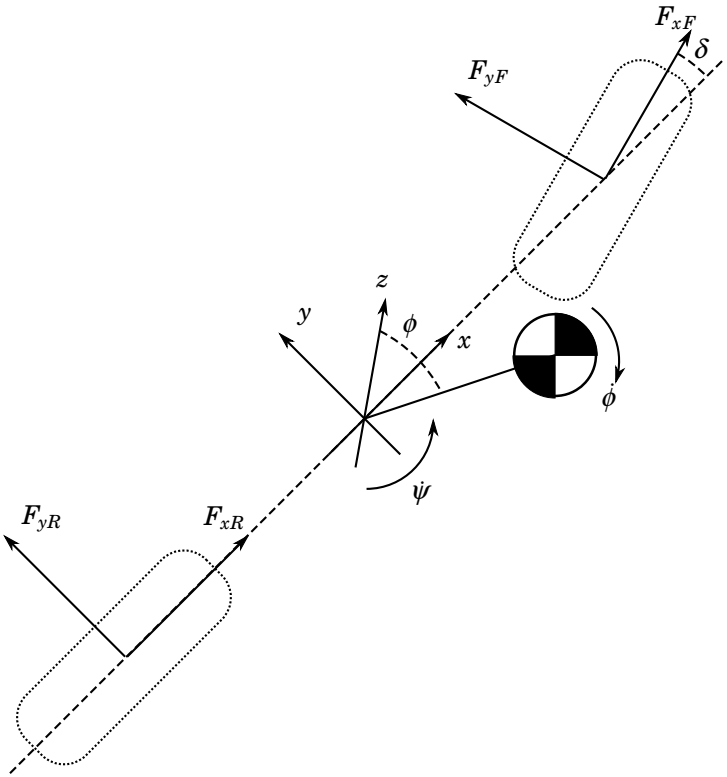

Figure 2.6 Single-track model with roll dynamics.

It should be noted that since the approximations made in the derivation of the model are based on the assumption of small steering angles, it may be necessary to perform some saturation of the outputs, based on the maximum available friction force.

Single-Track Model with Roll Dynamics

Roll dynamics and non-constant longitudinal velocity can be incorporated into a single-track model. The equations of motion are augmented

by a torque balance around the x axis. The equations are:

$$\begin{aligned} m(\dot{v} + u\dot{\psi}) &= F_{y,F} + F_{y,R} \\ I_{zz}\ddot{\psi} &= aF_{y,F} - bF_{y,R} \\ I_{xx}\ddot{\phi} + K_\phi\dot{\phi} + C_\phi\phi &= mh(\dot{v} + u\dot{\psi}) \end{aligned}$$

where K_ϕ and C_ϕ are damping and spring coefficients respectively. The slip angles are the same as in (2.10a), and the tire forces are considered to be linearly related to the slip angles as in (2.11a).

This model takes as inputs the steering angle δ and the longitudinal velocity u, and has roll angle ϕ, lateral velocity v, yaw rate $\dot{\psi}$ and vehicle sideslip angle β as outputs.

Two-Track Model

In order to incorporate the effects of the individual tire forces, as well as suspension and a more accurate representation of the roll dynamics, a two-track model can be used, shown in Figure 2.7. The suspension is modelled as a torsional spring and damper system acting around the roll axis, illustrated in Figure 2.8. In this way, the pitch dynamics of the vehicle are ignored. The resulting model has four degrees of freedom, namely translational motion along the x and y axis, as well as rotational motion about the x axis (roll) and the z axis (yaw).

Derivation of Tire Forces In the derivation of the model it will be convenient to express the tire forces acting on the vehicle as resultant forces in the x and y directions of the S_v frame as well as a resultant moment about the z axis. These forces and moments will be referred to as *generalized forces*. By considering Figure 2.9, the following expressions relating the individual tire forces to the generalized forces are obtained:

$$F_{xT} = F_x^{rl} + F_x^{rr} + (F_x^{fl} + F_x^{fr})\cos\delta - (F_y^{fl} + F_y^{fr})\sin\delta \tag{2.13a}$$

$$F_{yT} = F_y^{rl} + F_y^{rr} + (F_y^{fl} + F_y^{fr})\cos\delta + (F_x^{fl} + F_x^{fr})\sin\delta \tag{2.13b}$$

$$\begin{aligned} M_T = &(F_y^{fl} + F_y^{fr})a\cos\delta - (F_y^{rl} + F_y^{rr})b + (F_x^{fl} + F_x^{fr})a\sin\delta + \\ &(F_x^{rr} + F_x^{fr}\cos\delta + F_y^{fl}\sin\delta - F_x^{rl} - F_x^{fl}\cos\delta - F_y^{fr}\sin\delta)l \end{aligned} \tag{2.13c}$$

where δ is the steering angle (measured at the wheels).

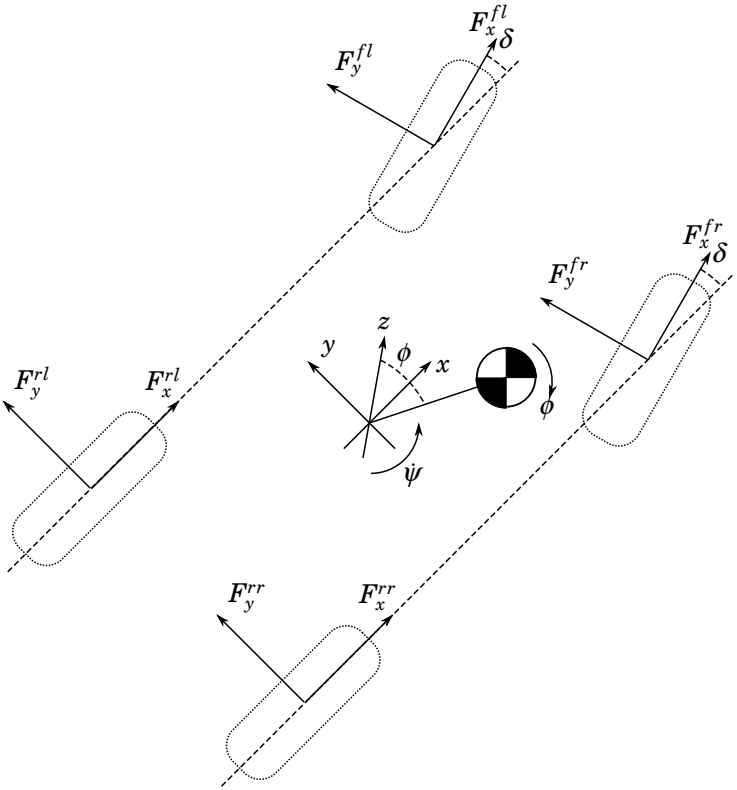

Figure 2.7 Two-track model with roll dynamics.

Newton-Euler Modeling

In this section a four degree of freedom model is derived using Newton-Euler modeling. The external forces acting on the vehicle are expressed in the vehicle coordinate system, so it is natural to write the equations of motion in this system.

Angular Motion Euler's equation states that the sum of the external torque acting on a system is given by the rate of change of angular

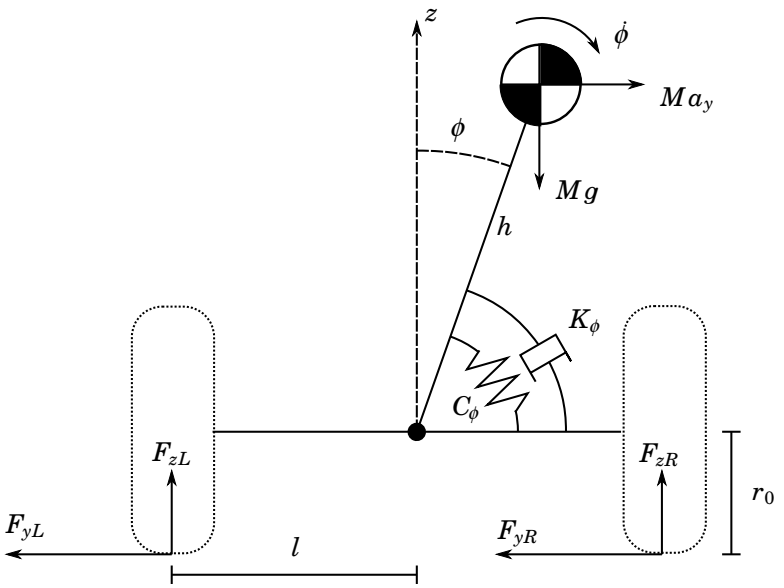

Figure 2.8 The two-track model in the vertical plane, showing suspension modeled as a torsional spring and damper.

momentum:

$$\tau = \frac{d(I^v \omega^s)}{dt} \tag{2.14}$$

where τ is the external torque or moment applied to the system, I^v is the inertia tensor relative to the coordinate frame in which the equations are to be derived, and ω^s is the spacial angular velocity.

Since the vehicle frame is rotating, it is not an inertial frame and (2.14) must be modified as in (2.8). The rate of change of angular momentum is given by:

$$\tau = \frac{d}{dt}(I^v \omega^s)\bigg|_v + \omega_i^v \times I^v \omega^s \tag{2.15}$$

where ω_i^v is the angular velocity of the vehicle coordinate system rel-

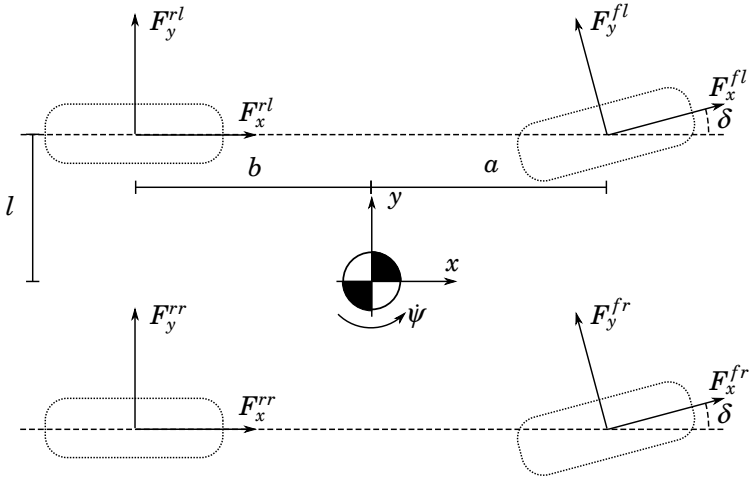

Figure 2.9 Planar chassis model, showing the horizontal components of the tire forces.

ative to the inertial system. This is given by:

$$\omega_i^v = \begin{pmatrix} 0 \\ 0 \\ \dot{\psi} \end{pmatrix} \tag{2.16}$$

The inertia tensor in the vehicle frame is given by:

$$I^v = R_b^v(\phi) I^b R_b^{v\,T}(\phi) \tag{2.17}$$

where I^b is the inertia tensor in the body frame:

$$I^b = \begin{pmatrix} I_{xx} & 0 & 0 \\ 0 & I_{yy} & 0 \\ 0 & 0 & I_{zz} \end{pmatrix} \tag{2.18}$$

This gives:

$$I^v = \begin{pmatrix} I_{xx} & 0 & 0 \\ 0 & I_{yy}\cos^2\phi + I_{zz}\sin^2\phi & (I_{yy} - I_{zz})\sin\phi\cos\phi \\ 0 & (I_{yy} - I_{zz})\sin\phi\cos\phi & I_{yy}\sin^2\phi + I_{zz}\cos^2\phi \end{pmatrix} \tag{2.19}$$

The spacial angular velocity ω_s is given by:

$$\omega_s = \begin{pmatrix} \dot{\phi} \\ 0 \\ \dot{\psi} \end{pmatrix} \tag{2.20}$$

The components of the torque vector which are of interest are the x and z components, given by:

$$\tau_x = F_{yT} h \cos\phi + mgh \sin\phi - C_\phi \phi - K_\phi \dot{\phi} \tag{2.21}$$
$$\tau_z = M_T - F_{xT} h \sin\phi \tag{2.22}$$

Using (2.15) the equations of angular motion are found to be:

$$\ddot{\phi} = \frac{F_{yT} h \cos\phi + mgh \sin\phi - C_\phi \phi - K_\phi \dot{\phi} + \dot{\psi}^2 (I_{yy} - I_{zz}) \sin\phi \cos\phi}{I_{xx}} \tag{2.23}$$

$$\ddot{\psi} = \frac{M_T - F_{xT} h \sin\phi - 2(I_{yy} - I_{zz}) \sin\phi \cos\phi \dot{\phi} \dot{\psi}}{I_{yy} \sin^2\phi + I_{zz} \cos^2\phi} \tag{2.24}$$

By assuming that the roll angle ϕ is small and making appropriate approximations, simplified expressions can be obtained:

$$\ddot{\phi} \approx \frac{F_{yT} h + mgh\phi - C_\phi \phi - K_\phi \dot{\phi} + \dot{\psi}^2 (I_{yy} - I_{zz}) \phi}{I_{xx}} \tag{2.25}$$

$$\ddot{\psi} \approx \frac{M_T - F_{xT} h\phi - 2(I_{yy} - I_{zz}) \phi \dot{\phi} \dot{\psi}}{I_{yy} \phi^2 + I_{zz}} \tag{2.26}$$

Translational Motion The equations for translational motion can be obtained from (2.9). The equations are:

$$\dot{u} = \frac{F_{xT}}{m} + v\dot{\psi} - h \sin\phi \ddot{\psi} \tag{2.27}$$

$$\dot{v} = \frac{F_{yT}}{m} - u\dot{\psi} - h \sin\phi \cos\phi \dot{\psi}^2 + h\ddot{\phi} \tag{2.28}$$

Substituting the expressions for the angular accelerations from (2.23) and (2.24) into (2.27) and (2.28) gives:

$$\dot{u} = \frac{F_{xT}}{m} + v\dot{\psi} - h\sin\phi\left(\frac{M_T - F_{xT}h\sin\phi - 2(I_{yy} - I_{zz})\sin\phi\cos\phi\dot{\phi}\dot{\psi}}{I_{yy}\sin^2\phi + I_{zz}\cos^2\phi}\right) \tag{2.29}$$

$$\dot{v} = \frac{F_{yT}}{m} - u\dot{\psi} - h\sin\phi\cos\phi\dot{\psi}^2 + \frac{h}{I_{xx}}(F_{yT}h\cos\phi + mgh\sin\phi - C_\phi\phi - K_\phi\dot{\phi} + \dot{\psi}^2(I_{yy} - I_{zz})\sin\phi\cos\phi) \tag{2.30}$$

The translational and angular equations of motion are thus given by (2.29), (2.30), (2.23) and (2.24). The angular equations are of primary interest for control purposes.

Euler-Lagrange Modeling

In this section, the Euler-Lagrange method will be used to obtain the equations of motion for the four degree of freedom vehicle model, including a constant but nonzero pitch angle θ_r. The derivation follows that in [Pacejka, 2002]. The Euler-Lagrange equations state that:

$$\frac{d}{dt}\frac{\partial T}{\partial \dot{q}_i} - \frac{\partial T}{\partial q_i} + \frac{\partial U}{\partial q_i} = Q_i \tag{2.31}$$

where T is the kinetic energy of the system, U is the potential energy, q_i are generalized coordinates and Q_i are generalized forces corresponding to the generalized coordinates.

An obvious choice of coordinates for the system are the X and Y coordinates of the ground-fixed (inertial) coordinate system, the yaw angle ψ between the X axis and the (vehicle-fixed) x axis, and the roll angle ϕ, defined around the vehicle's roll axis. However, when dealing with larger values of ϕ, it is often preferred to use a different choice of variables, namely the longitudinal and lateral velocities u and v, as well as the yaw rate $\dot{\psi}$ and roll angle ϕ. Since the coordinates x and y cannot be found by integrating the velocities u and v, the Lagrange equations in this case must be modified. It can be shown that the

resulting equations are:

$$\frac{d}{dt}\frac{\partial T}{\partial u} - \dot{\psi}\frac{\partial T}{\partial v} = Q_u \tag{2.32a}$$

$$\frac{d}{dt}\frac{\partial T}{\partial v} + \dot{\psi}\frac{\partial T}{\partial u} = Q_v \tag{2.32b}$$

$$\frac{d}{dt}\frac{\partial T}{\partial \dot{\psi}} - v\frac{\partial T}{\partial u} + u\frac{\partial U}{\partial v} = Q_{\dot{\psi}} \tag{2.32c}$$

$$\frac{d}{dt}\frac{\partial T}{\partial \dot{\phi}} - \frac{\partial T}{\partial \phi} + \frac{\partial U}{\partial \phi} = Q_\phi \tag{2.32d}$$

The generalized forces Q_i can be obtained from the expression for virtual work:

$$\delta W = \sum_{i=1}^{4} Q_i \delta q_i$$

Here, q_i refer to the 'quasi-coordinates' x and y, as well as the real coordinates ϕ and ψ. The term 'quasi-coordinate' is used because we cannot obtain x and y by integrating u and v.

For our system the virtual work is given by:

$$\delta W = \sum F_x \delta x + \sum F_y \delta y + \sum M_z \delta \psi + \sum M_\phi \delta \phi$$

The generalized forces are given by (2.13):

$$\sum F_x = F_{xT} \tag{2.33a}$$

$$\sum F_y = F_{yT} \tag{2.33b}$$

$$\sum M_z = M_T \tag{2.33c}$$

$$\sum M_\phi = -K_\phi \dot{\phi} \tag{2.33d}$$

In the last equation K_ϕ is the damping coefficient, representing the dampers in the suspension.

The kinetic and potential energies must now be derived. The kinetic energy is composed of two parts, the translational part and the

rotational part. The velocities of the centre of gravity in the x and y directions are given by:

$$u_{CG} = u - h \sin\phi\dot{\psi}$$
$$v_{CG} = v + h\dot{\phi}$$

where h is the distance of the centre of gravity from the roll axis. Here, the angle θ_r between the roll axis and the x axis is neglected. The translational kinetic energy is therefore given by (with θ_r neglected and ϕ assumed small):

$$T_{trans} = \frac{1}{2}m\big((u - h\phi\dot{\psi})^2 + (v + h\dot{\phi})^2\big)$$

The rotational kinetic energy of a system is given by [Spiegel, 1967]:

$$T_{rot} = \frac{1}{2}\Big(I_{xx}\omega_x^2 + I_{yy}\omega_y^2 + I_{zz}\omega_z^2 + 2I_{xy}\omega_x\omega_y + 2I_{xz}\omega_x\omega_z + 2I_{yz}\omega_y\omega_z\Big)$$

where I_{ii} are the moments of inertia around the axis i and the quantities I_{ij} are products of inertia.

According to [Pacejka, 2002], the rotational kinetic energy of the system (with θ_r accounted for but assumed small, and ϕ also assumed small) is given by:

$$T_{rot} = \frac{1}{2}\Big(I_{xx}\dot{\phi}^2 + I_{yy}(\phi\dot{\psi})^2 + I_{zz}(\dot{\psi}^2 - \phi^2\dot{\psi}^2 + 2\theta_r\dot{\psi}\dot{\phi}) - 2I_{xz}\dot{\psi}\dot{\phi}\Big)$$

The total kinetic energy is obtained by summing the two parts:

$$T = \frac{1}{2}m\big((u - h\phi\dot{\psi})^2 + (v + h\dot{\phi})^2\big) + \tag{2.34}$$
$$+ \frac{1}{2}\Big(I_{xx}\dot{\phi}^2 + I_{yy}(\phi\dot{\psi})^2 + I_{zz}(\dot{\psi}^2 - \phi^2\dot{\psi}^2 + 2\theta_r\dot{\psi}\dot{\phi}) - 2I_{xz}\dot{\psi}\dot{\phi}\Big)$$

The potential energy of the system is stored in the suspension springs and the height of the centre of gravity. It is given by:

$$U = \frac{1}{2}C_\phi\phi^2 - mg(h - h\cos\phi)$$

If a small angle approximation is used for the second term on the right hand side, the term will disappear. Instead, write:

$$\begin{aligned} mgh(1-\cos\phi) &= 2mgh\sin^2\left(\frac{\phi}{2}\right) \\ &\approx \frac{1}{2}mgh\phi^2 \end{aligned}$$

The potential energy is then given by:

$$U = \frac{1}{2}C_\phi\phi^2 - \frac{1}{2}mgh\phi^2$$

The equations of motion may now be obtained by evaluating the Lagrangian equations. To evaluate (2.32a) the following partial derivatives must first be calculated:

$$\begin{aligned} \frac{\partial T}{\partial u} &= m(u - h\phi\psi) & \frac{\partial T}{\partial v} &= m(v + h\dot{\phi}) \\ \frac{d}{dt}\frac{\partial T}{\partial u} &= m\dot{u} - mh(\dot{\phi}\psi + \phi\dot{r}) \end{aligned}$$

The first equation of motion is then given by:

$$m\left[\dot{u} - \psi v - h(2\dot{\phi}\psi + \phi\ddot{\psi})\right] = F_{xT} \tag{2.35}$$

To derive the next equation the derivative:

$$\frac{d}{dt}\frac{\partial T}{\partial v} = m\dot{v} + mh\ddot{\phi}$$

must be calculated. The second equation of motion is then:

$$m\left[\dot{v} + \dot{\psi}u + h(\ddot{\phi} - \dot{\psi}\phi)\right] = F_{yT} \tag{2.36}$$

For the third equation the derivatives:

$$\begin{aligned} \frac{\partial T}{\partial \dot{\psi}} &= -mhu\phi + mh^2\phi^2\dot{\psi} + I_{yy}\phi^2\dot{\psi} + I_{zz}(\dot{\psi} - \dot{\psi}\phi^2 + \theta_r\dot{\phi}) - I_{xz}\dot{\phi} \\ \frac{d}{dt}\frac{\partial T}{\partial \dot{\psi}} &= -mh\dot{u}\phi - mhu\dot{\phi} + (mh^2 + I_{yy})[\ddot{\psi}\phi^2 + 2\dot{\psi}\phi\dot{\phi}] + \\ &\quad + I_{zz}(\ddot{\psi} - \ddot{\psi}\phi^2 - 2\dot{\psi}\phi\dot{\phi} + \theta_r\ddot{\phi}) - I_{xz}\ddot{\phi} \end{aligned}$$

are calculated.The third equation of motion is given by:

$$I_{zz}\dot{r} - mh(\dot{u} - \psi v)\phi + (I_{zz}\theta_r - I_{xz})\ddot{\phi} = M_T \tag{2.37}$$

For the fourth equation of motion the partial derivatives with respect to ϕ must be calculated:

$$\begin{aligned}
\frac{\partial T}{\partial \dot{\phi}} &= mh(v + h\dot{\phi}) + I_{xx}\dot{\phi} + I_{zz}\theta_r\dot{\psi} - I_{xz}\dot{\psi} \\
\frac{\partial T}{\partial \phi} &= -mh\dot{\psi}(u - h\phi\dot{\psi}) + I_{yy}\dot{\psi}^2\phi - I_{zz}\dot{\psi}^2\phi \\
\frac{\partial U}{\partial \phi} &= C_\phi\phi - mgh\phi \\
\frac{d}{dt}\frac{\partial T}{\partial \phi} &= mh(\dot{v} + h\ddot{\phi}) + I_{xx}\ddot{\phi} + I_{zz}\theta_r\ddot{\psi} - I_{xz}\ddot{\psi}
\end{aligned}$$

The final equation of motion is then given by:

$$\begin{aligned}
&(I_{xx} + mh^2)\ddot{\phi} + mh(\dot{v} + \dot{\psi}u) + (I_{zz}\theta_r - I_{xz})p\ddot{s}i - (I_{yy} + mh^2 - I_{zz})\dot{\psi}^2\phi \\
&+ (C_\phi - mgh)\phi - K_\phi\dot{\phi} = 0
\end{aligned} \tag{2.38}$$

The model can be written on the form:

$$\begin{aligned}
&\begin{pmatrix}
m & 0 & -mh\phi & 0 & 0 \\
0 & m & 0 & mh & 0 \\
-mh\phi & 0 & I_{zz} & I_{zz}\theta_r - I_{xz} & 0 \\
0 & mh & I_{zz}\theta_r - I_{xz} & I_{xx} + mh^2 & K_\phi \\
0 & 0 & 0 & 0 & 1
\end{pmatrix}
\begin{pmatrix}
\dot{v_x} \\ \dot{v_y} \\ \ddot{\psi} \\ \ddot{\phi} \\ \dot{\phi}
\end{pmatrix} \\
&= \begin{pmatrix}
F_{xT} + m\dot{\psi}v + 2mh\dot{\phi}\dot{\psi} \\
F_{yT} - m\dot{\psi}u + mh\dot{\psi}^2\phi \\
M_T - mhv\dot{\psi}\phi \\
-mhu\dot{\psi} + (mh^2 + I_{yy} - I_{zz})\dot{\psi}^2\phi - (C_\phi - mgh)\phi \\
\dot{\phi}
\end{pmatrix}
\end{aligned} \tag{2.39}$$

The parameters of the two-track models are summarized in Table 2.1.

Symbol	Description
m	Vehicle mass
h	Height of CG above roll axis
I_{xx}	Moment of inertia about x–axis
I_{yy}	Moment of inertia about y–axis
I_{zz}	Moment of inertia about z–axis
I_{xz}	Product of inertia for x and z axes
a	Distance from front axle to CG position (along x–axis)
b	Distance from rear axle to CG position (along x–axis)
l	Half track width
C_ϕ	Total roll stiffness
K_ϕ	Total roll damping
θ_r	Angle between roll axis and x–axis

Table 2.1 Parameters of the two–track model

Application of Models

Reference Trajectory Generation The linear bicycle model described in Section 2.3 is not sufficient for control design since it lacks roll behavior. However, it may be used for the generation of reference trajectories, in particular the generation of a yaw rate reference, given the driver's steering command δ and the vehicle's longitudinal velocity.

Models for Control Design A linear model including roll dynamics could be used for roll control, and linear models are indeed extensively used in the literature. However, linear models use a number of assumptions and approximations which are unlikely to be valid during extreme maneuvering. These include:

- Constant longitudinal velocity
- Small steering angles
- Linear tire forces

- Simple approximations of tire slip values (α)

These approximations imply that although linear models may be useful for designing control systems intended for use under 'normal' driving conditions, they may be of limited use for the case of extreme maneuvering, where nonlinearities in tire characteristics and vehicle dynamics must be taken into account. In addition, the load transfer which occurs during extreme maneuvering cannot be modeled with a single-track model. For these reasons, the two-track nonlinear model given in (2.23), (2.24), (2.27) and (2.28) will be used as a basis for control design.

3

Rollover Analysis and Detection

3.1 Introduction

In this chapter, analysis of the vehicle rollover phenomenon is performed. The aim of the analysis is to give insight into the mechanisms that cause rollover, and to determine how detection of an imminent rollover event should be performed. The chapter begins with simple static analysis, including simple stability analysis. Methods of rollover detection are then discussed, including a review of previous work.

3.2 Static Rollover Analysis

The underlying cause of untripped vehicle rollover accidents is the rotational motion occurring when a vehicle makes a turn. Figure 3.1 illustrates a vehicle performing a turn with a radius of curvature ρ. In order to maintain the curved trajectory, a force directed towards the centre of rotation must act upon the centre of gravity (CG) of the vehicle. Another way of considering this is to use the method of D'Alembert [Spiegel, 1967], in which accelerations are represented by pseudo-forces. D'Alembert's method allows dynamics problems to be viewed as statics problems. Figure 3.2 shows the pseudo-force ma_y

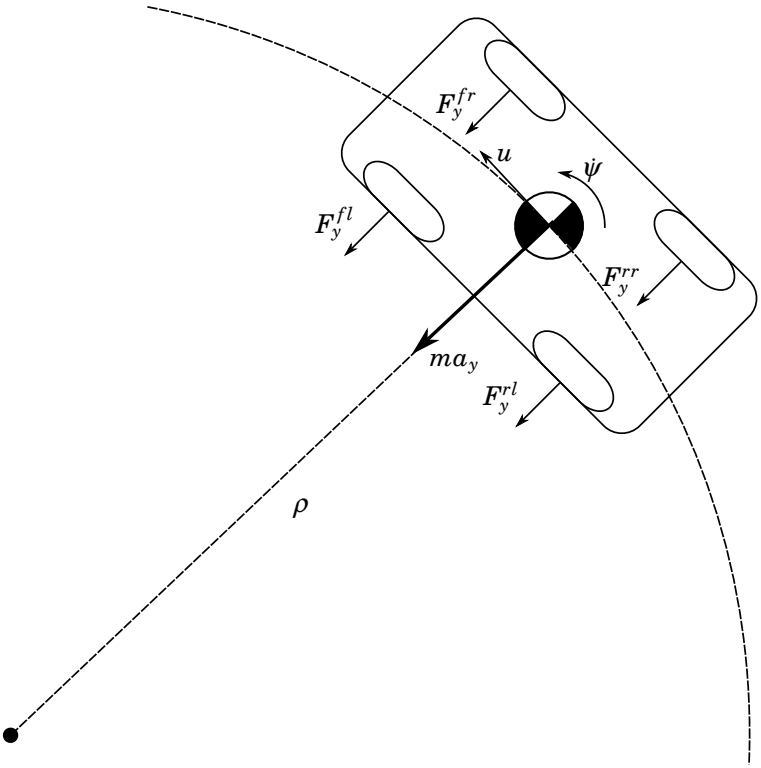

Figure 3.1 Illustration of a vehicle driving along a curved trajectory with radius of curvature ρ.

acting on the centre of gravity of a vehicle performing a turn. Note that the pseudo-force acts in the opposite direction to the acceleration that it replaces, that is, it is directed radially outwards from the centre of rotation. The external forces acting on the vehicle act at the road-tire contact point, not the centre of gravity, meaning that a resulting moment acts on the vehicle. The magnitude of the resulting moment depends on the height of the centre of gravity above the road. A higher centre of gravity gives a larger moment. This moment is counteracted by a moment due to the reaction (normal) forces acting on the tires

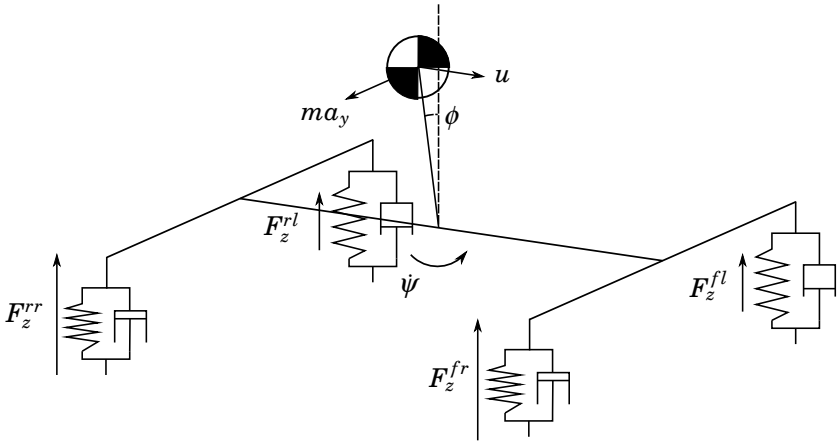

Figure 3.2 Illustration of the pseudo-force ma_y acting on the vehicle's centre of gravity.

on the outside of the turn. This moment depends on the track width of the vehicle (the distance between inner and outer wheels). Clearly, if the moment due to the rotational motion of the vehicle exceeds the moment due to the the normal forces on the tires, then the vehicle will begin to roll.

A static condition for rollover can be derived from consideration of the resultant force vector acting on the center of gravity. If the line of action of the force lies outside the contact point of the outside wheels, then rollover will occur. Figure 3.3 illustrates the situation in the case of a vehicle without suspension. In this case, the condition for rollover to occur is:

$$\begin{aligned} ma_y h_T &> mgl \\ a_y &> \frac{gl}{h_T} \end{aligned} \tag{3.1}$$

It is easy to see from (3.1) that the ratio of the height of the centre of gravity h_T to track width l determines the lateral acceleration necessary for rollover to occur. It is also worthy of note that the vehicle mass m does not appear in the condition. Only the geometry of the vehicle

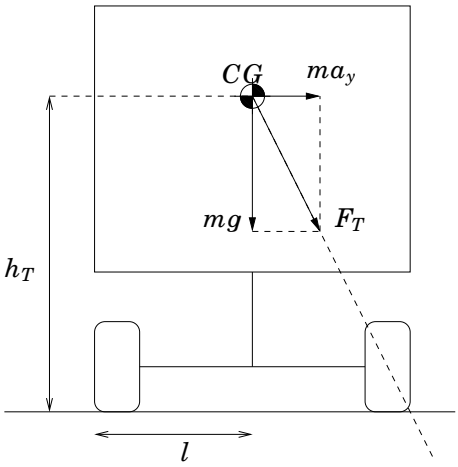

Figure 3.3 Illustration of the rollover limit for a vehicle with suspension elements neglected. The line of action of the resultant force acting on the CG passes through the contact point of the tires on the outside of the turn.

is important. Figure 3.4 illustrates the slightly more complicated case of a vehicle in which suspension elements are taken into account. In this case the condition for rollover to occur is given by:

$$a_y > \frac{g(l - h_T \sin\phi)}{h_T \cos\phi} \tag{3.2}$$

3.3 Stability

When the lateral acceleration threshold (3.1) obtained from analysis of Figure 3.3 is exceeded, roll motion of the vehicle ensues. Figure 3.5 illustrates the simple case of a vehicle without suspension after the onset of rollover. To gain insight into the nature of rollover accidents, it is interesting to perform some stability analysis for this simplified model. By resolving the weight mg and the pseudo-force ma_y into components in the vehicle-fixed y and z directions, the following dynamics

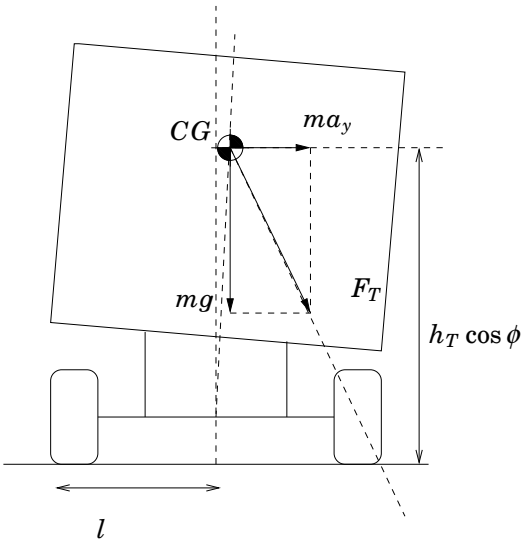

Figure 3.4 Illustration of the rollover limit for a vehicle with suspension elements taken into account. The changing position of the CG implies that the lateral acceleration required to produce rollover becomes smaller for larger roll angles.

are obtained:

$$m(a_y l \sin\phi + a_y h \cos\phi + gh \sin\phi - gl \cos\phi) = I\ddot{\phi} \qquad (3.3)$$

It is clear from (3.3) that the resultant roll moment becomes larger as the roll angle ϕ increases. Figure 3.6 shows the variation of the overturning moment with roll angle for a number of different values of the lateral acceleration. The parameters used in the plots were $m =$ 3500kg, $h = 1.4$m and $l = 0.9$m.

Although this analysis is based on a very simple model, ignoring the dynamic effects of the suspension, it brings to light some important points. Primarily, it can be seen that large sustained lateral accelerations are not necessary to cause rollover. Once rollover has begun, the magnitude of the lateral acceleration required to sustain it decreases. The effect of the lateral acceleration is replaced by the component of the weight acting along the vehicle's y axis.

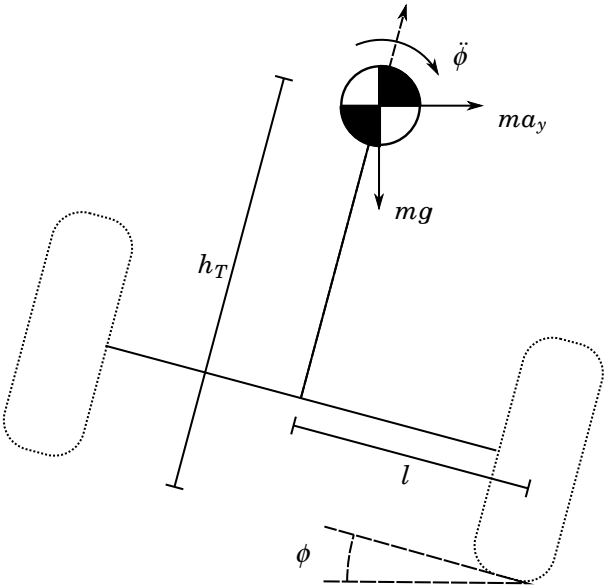

Figure 3.5 Illustration of vehicle after the onset of rollover.

3.4 Load Transfer

An important phenomenon in the study of rollover is load transfer. Load transfer refers to the shift in distribution of the vehicle's weight between the wheels. This has an important effect on the forces acting on the vehicle, due to the fact that the maximum achievable friction force for each tire depends on the normal force acting on the tire.

Lateral Load Transfer

Lateral load transfer is the change in normal force acting on the tires due to both the acceleration of the centre of gravity, and the shifting of position of the CG in the y direction due to the movement of the suspension. Figure 3.7 illustrates lateral load transfer in the vertical plane. Figure 3.2 shows the effect of load transfer on the suspension.

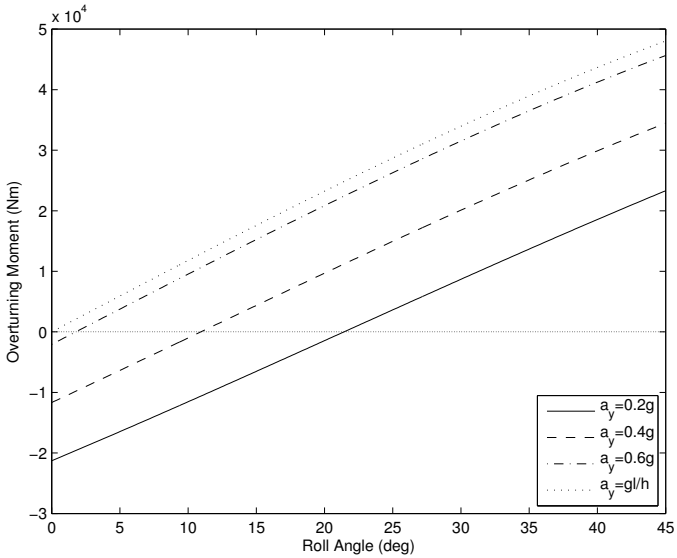

Figure 3.6 Plot showing the variation of the resulting moment acting on the vehicle with roll angle for different values of the lateral acceleration a_y.

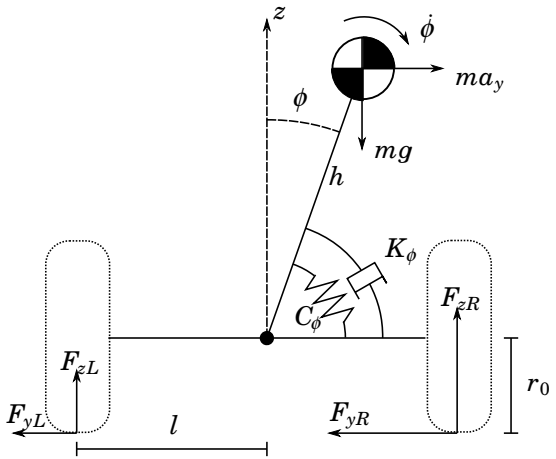

Figure 3.7 Lateral load transfer illustrated in the vertical plane.

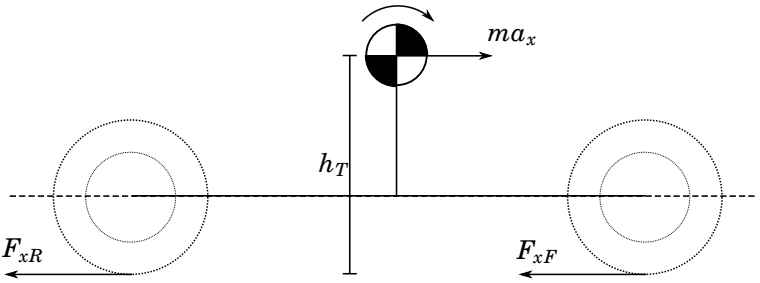

Figure 3.8 Illustration of longitudinal load transfer during braking.

Longitudinal Load Transfer

In addition to lateral load transfer, longitudinal load transfer can occur, due to acceleration in the longitudinal direction. Longitudinal load transfer occurs between the front and rear axles of the vehicle. The total resultant load transfer for each tire is the sum of the lateral and longitudinal load transfer. Figure 3.8 illustrates longitudinal load transfer. The simultaneous effect of lateral and longitudinal load transfer is illustrated in Figure 3.9.

Load Transfer Ratio

The load transfer ratio (LTR) can be defined as the difference between the normal forces on the right and left hand sides of the vehicle divided by their sum:

$$\mathrm{R} = \frac{F_{zR} - F_{zL}}{F_{zR} + F_{zL}} \tag{3.4}$$

where R denotes the LTR. Assuming no vertical motion, the sum of the normal forces equals the weight of the vehicle:

$$\mathrm{R} = \frac{F_{zR} - F_{zL}}{mg} \tag{3.5}$$

The LTR is defined for the entire vehicle. However, it is important to note that the longitudinal load transfer has the effect of decreasing the normal forces at the rear wheels during cornering (this is true even if

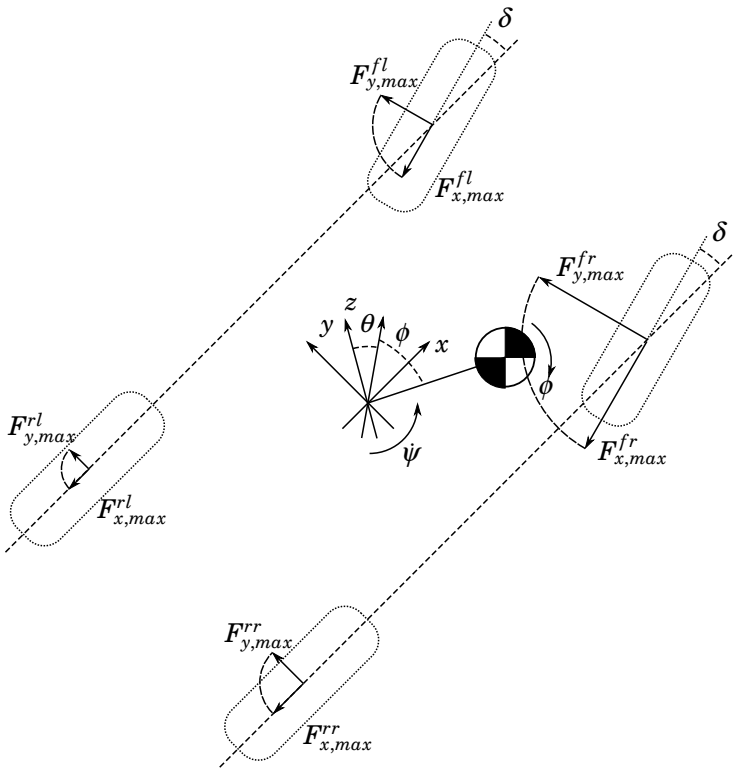

Figure 3.9 Illustration of the effects of load transfer on attainable tire forces during simultaneous cornering and braking.

braking is not performed, since the lateral forces have a component in the negative x direction). This effect implies that the rear wheel on the inside of the turn will be the first to lose contact with the road during a rollover.

3.5 Methods for Rollover Detection

Vehicle dynamics controllers do not operate continuously. They are typically activated only for certain situations. This switching requires

some form of algorithm capable of detecting when the vehicle has entered, or is about to enter, a state in which the controller should be active. For VDC systems dealing with rollover prevention, the switching algorithm must be capable of detecting when a rollover is imminent. As was shown in the preceding section, the vehicle becomes increasingly unstable during rollover. It is therefore desirable that the detection algorithm has some form of predictive action, so that the controller may be activated as rapidly as possible.

A number of methods for rollover detection have been suggested in the literature, and some have been implemented in production vehicles. This section summarises a number of approaches to rollover detection. A more in-depth review of rollover detection methods can be found in [Dahlberg, 2001].

Roll Angle and Roll Rate Measurement

If the vehicle is equipped with sensors capable of measuring the roll angle ϕ and roll rate $\dot{\phi}$, rollover detection can be performed simply by analysing these measurements. The simplest approach would be to define a threshold value of the roll angle ϕ_{max} and to switch on the controller when $|\phi| > \phi_{max}$. In order to introduce predictive action to the algorithm, the roll rate measurement may be used. For instance, the controller may be switched on when $|\phi| > \phi_{max}$ and $\dot{\phi}\text{sign}(\phi) > 0$. An obvious disadvantage using roll angle and roll rate measurements is that extra sensors are required.

Load Transfer-based Methods

Since load transfer occurs in connection with rollover events, the load transfer ratio is often used for rollover detection as well as control. The case of $R = \pm 1$, corresponding to the point at which one wheel begins to lose contact with the road surface, is often used as a 'critical situation' which should be avoided in order to prevent rollover [Odenthal *et al.*, 1999; Johansson and Gäfvert, 2004]. The load transfer ratio R is used as the switching variable in [Odenthal *et al.*, 1999], in which emergency braking is used to mitigate rollover. Two switching algorithms are proposed. One is based on a threshold value of R, denoted

$\hat{R}$, and results in the control law:

$$F_{xT} = \begin{cases} 0 & \text{if } |R| \leq \hat{R} \\ -ma_{x,max} & \text{if } |R| > \hat{R} \end{cases} \tag{3.6}$$

where F_{xT} is the total braking force and $a_{x,max}$ is the maximum allowed deceleration. A dynamic switching strategy is also proposed, based on the derivative of the load transfer ratio. The idea is that the controller should be fully active when R is greater than $\hat{R}$ and is increasing ($\dot{R}\text{sign}(R) > 0$) , but should be gradually switched off when R is decreasing ($\dot{R}\text{sign}(R) < 0$). This results in the control law:

$$F_{xT} = \begin{cases} 0 & \text{if } |R| \leq \hat{R} \\ -ma_{x,max} & \text{if } |R| > \hat{R} \text{ and } \dot{R}\text{sign}(R) > 0 \\ -\dfrac{|R| - \hat{R}}{R_{max} - \hat{R}} ma_{x,max} & \text{if } |R| > \hat{R} \text{ and } \dot{R}\text{sign}(R) < 0 \end{cases} \tag{3.7}$$

Energy-based Methods

The detection of a rollover event, and the subsequent activation of the controller, can be performed by considering the roll energy of the vehicle. The 'critical situation' is defined as when two wheels begin to lift from the ground, that is, the normal forces for these wheels become zero. In this situation, complete load transfer occurs, meaning that the total normal force on the side of the vehicle remaining in contact with the ground is equal to the vehicle's weight mg. It is assumed that the total lateral tyre force F_{yT} for the wheels retaining contact are at their maximum levels, so that $F_{yT} = \mu F_{zT} = \mu mg$.

The roll energy associated with the vehicle is composed of a potential energy part involving the energy stored in the suspension springs as well as the height of the center of gravity, and a kinetic energy part. The roll energy is given by:

$$E = \frac{1}{2} C_\phi \phi^2 - mgh(1 - \cos\phi) + \frac{1}{2}(I_{xx} + mh^2)\dot{\phi}^2 \tag{3.8}$$

A critical value of the roll energy, $E_{critical}$ can now be found, which represents the minimum possible roll energy in the critical situation of wheel lift-off.

For rollover to occur, the total moment around the roll axis due to the motion of the center of gravity must be greater than the moment due to the normal force from the tyres still in contact. The critical situation can then be defined by an inequality involving moments acting on the vehicle.

$$F_{zT} l < F_{yT} r_0 + C_\phi \phi + K_\phi \dot{\phi} \tag{3.9}$$

The critical roll energy $E_{critical}$ is found by minimizing (3.8) over ϕ and $\dot{\phi}$, subject to (3.9) (with the inequality replaced by an equality).

In [Johansson and Gäfvert, 2004], a normalized rollover warning (ROW) measure is introduced, defined as:

$$ROW = \frac{E_{critical} - E}{E_{critical}}$$

The critical situation can thus be reached for $ROW \leq 0$. Switching is then accomplished by setting a threshold value of ROW (greater than zero),which can be found experimentally, and switching on the controller when $ROW \leq ROW_{threshold}$.

Lateral Acceleration-based Methods

As has been indicated in this chapter, the root cause of the rollover problem can be seen as the D'Alembert pseudo-force ma_y acting at the centre of gravity and giving rise to a roll moment. Since the lateral acceleration a_y is usually measured in vehicles equipped with ESP systems, its use in rollover detection is attractive. The lateral acceleration limits (3.1) and (3.2) could be used as a starting point for obtaining a switching algorithm based on the lateral acceleration measurement. However, these limits are based on greatly simplified models. The limit in (3.2), obtained from a slightly more complex model that the limit in (3.1), gives a lower value for the maximum allowable lateral acceleration. Increasing the complexity of the model will in general result in increasingly smaller values. In addition, the situation becomes more complex when the suspension dynamics are accounted for. In this case, the state of the vehicle suspension system determines the rollover threshold. This is easily explained in physical terms; when the vehicle begins a turn at a time when the suspension is in steady state, energy

is stored in the springs and more lateral acceleration is required for rollover. On the other hand, if energy is stored in the springs, and the vehicle is then subject to an acceleration in the opposite direction, the subsequent release of energy from the suspension will result in a lower value of lateral acceleration required for rollover. The lateral acceleration could be used in either a threshold-based switching strategy or a dynamic one. A threshold-based strategy could take the form:

$$F_{xT} = \begin{cases} 0 & \text{if } |a_y| \leq a_{y,threshold} \\ -ma_{x,max} & \text{if } |a_y| > a_{y,threshold} \end{cases} \tag{3.10}$$

which is similar to (3.6). A dynamic switching strategy could take a form similar to (3.7). However, care should be taken when implementing the time derivative of measured signals. The presence of noise means that filtering must be performed. To approach the problem more rigorously, the detection algorithm can be considered in the context of PD control.

PD Control A proportional-plus-derivative (PD) controller can be described by:

$$u(t) = K\left(e(t) + T_d \frac{de(t)}{dt}\right) \tag{3.11}$$

where $u(t)$ is the control signal and $e(t)$ is the tracking error. The derivative time constant T_d can be interpreted as the prediction horizon of the controller. In practice, (3.11) cannot be implemented directly because the derivative action greatly amplifies the noise. A common modification is to introduce a low-pass element into the transfer function for the derivative part. This may be seen as approximating the original transfer function:

$$sT_d \approx \frac{sT_d}{1 + sT_d/N} \tag{3.12}$$

where N is a parameter used to limit the high frequency gain.

A PD structure may be used to obtain a switching condition. Let $\hat{a}_y(t)$ denote the signal on which the switching is performed. Using the

modified PD law, $\hat{a}_y(t)$ may be obtained using the filter:

$$\hat{A}_y(s) = K\left(A_y(s) + \frac{sT_d}{1 + sT_d/N}A_y(s)\right) \tag{3.13}$$

where $A_y(s)$ and $\hat{A}_y(s)$ are the Laplace transforms of $a_y(t)$ and $\hat{a}_y(t)$ respectively. This can be seen as a predicted value of a_y in T_d seconds in the future when $K = 1$. A switching law could then take the form:

$$F_{xT} = \begin{cases} 0 & \text{if } |\hat{a}_y(t)| \leq a_{y,threshold} \\ -ma_{x,max} & \text{if } |\hat{a}_y(t)| > a_{y,threshold} \end{cases} \tag{3.14}$$

Dynamic or predictive switching of this type may be useful for compensating for actuator dynamics. For example, braking systems typically have rate constraints which means that desired braking forces are not reached until after a certain rise time. The derivative time constant T_d may be used to compensate for these dynamics.

Summary

In this section a number of methods for rollover detection have been reviewed. In selecting an appropriate method it is necessary to take into account not only the potential effectiveness of the method but also practical considerations such as the availability of the information required by the algorithms. Algorithms based on energy and load transfer, for instance, require either measurements or good estimates of a number of variables. In addition,a number of vehicle parameters are required for the energy-based methods. Apart from these considerations, it is possible to group the methods into ‘cause-based’ and ‘effect-based’ methods. Energy considerations and load transfer can be seen as effects of a rollover event, while lateral acceleration may be seen as the cause. For these reasons, the methods of detection based on lateral acceleration are chosen for use in the switching algorithm. In the following chapter control designs based on these methods will be developed.

4

Controller Design

4.1 Introduction

As can be seen from Chapter 2, the equations governing the vehicle dynamics and tire characteristics are complex. The plant can be considered as a nonlinear multiple-input multiple-output (MIMO) plant with a number of important input constraints. These constraints are due to the limitations of the actuators (only negative forces may be applied) as well as the complex tire characteristics. Any control strategy must handle these constraints explicitly. Figure 4.1 illustrates the structure of the vehicle models derived in Chapter 2.

Control Allocation: Motivation

In traditional control design, the control signal is assumed to be the actual input to the system. This input could be a valve position, a voltage or current, or any number of other physical quantities. Although this assumption is reasonable in most cases, there exist control design tasks which are less well suited to this approach. This is particularly true in the case of vehicle control. Road vehicles, aircraft and ships typically have large number of actuators, which often affect the vehicles' dynamics in complex ways. Aircraft have many control surfaces which can be used in different ways to produce movement.

A key issue is redundancy: the same control action can be produced in many different ways using different combinations of the actuators.

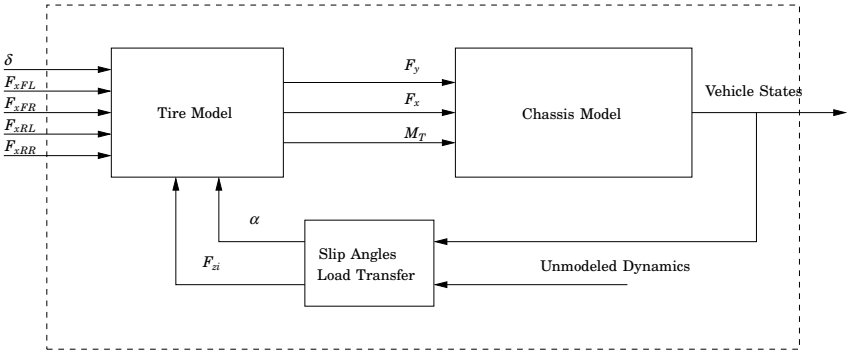

Figure 4.1 Block diagram representation of the two-track vehicle model, consisting of a tire model and a chassis model. The actuator inputs are the four braking forces, as well as the steering angle. The outputs of the system are the vehicle states.

It is clear that the 'control action' being referred to here is some abstract quantity. Because of this it is attractive to perform control design based on control signals which are not the same as the actual inputs to the system. For model-based control design, it is often easier to work with models describing the response of the system to external forces and moments, rather than actuator positions or voltages. In the aircraft example, the dynamic model of the system uses resultant forces and moments acting on the aircraft, rather than actuator positions. In vehicle control for instance it is very common to use resultant forces and moments acting on the vehicle as control signals, rather than actuator positions. The control design task is effectively split into two parts. In the first part, standard control design methods are used to obtain 'virtual' control signals. The second part consists of transforming these virtual control signals into actual control signals which may be applied to the process to be controlled. This is illustrated in Figure 4.2, in which the controller generates the virtual controls v, which are transformed by the control allocator into actual controls u

Although the mapping between actuator inputs and generalized forces and moments may usually be considered static, there are a number of good reasons for not using the actual control signals directly.

Control allocation is typically used for over-actuated systems, in

which there are more actuator inputs than 'virtual' control inputs. Returning to the aircraft example, the virtual controls or generalized forces consist of three forces and three moments. However, depending on the aircraft configuration, there may be a large number of different actuators which may be used to obtain these resultant forces and moments. These could include elevators, ailerons, canard foreplanes, thrust vectoring and more. Similarly, for a road vehicle, resultant forces and moments may be achieved by using individual wheel braking, active steering, and active suspension. This is illustrated in Figure 4.3. Additional complications arise when constraints are imposed on the actuators, as is practically always the case in applications. In this case the control allocator must choose a combination of actuator inputs which give the desired result while satisfying the constraints. Control allocation will be studied in more detail in Chapter 5.

4.2 Control Strategy

The control task consists of two parts. Primarily, vehicle rollover must be prevented. Secondly, the yaw rate must be stabilized, and should track a reference. This secondary control objective is important, since the extreme maneuvering giving rise to a potential rollover may be necessary to avoid an obstacle, or remain on the road. Restriction of the vehicle sideslip angle β (the angle between the vehicle-fixed x-axis and the velocity vector) is also important, but this can be accomplished through appropriate yaw rate control [Tøndel and Johansen, 2005].

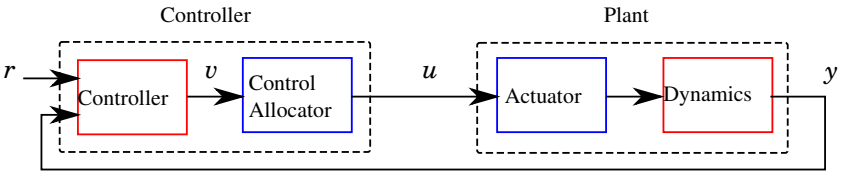

Figure 4.2 Control system structure with control allocation. The plant is split up into an actuator part and a dynamics part. The controller is similarly split into a controller which generates the virtual controls v, and a control allocator, which maps the virtual controls to actual controls u.

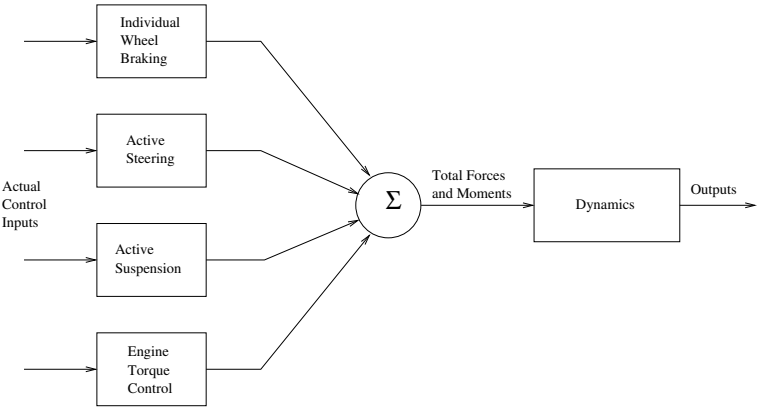

Figure 4.3 Block diagram illustrating the separation of actuator contributions and vehicle dynamics.

For the design, the generalized forces and moments, or virtual controls $v = \begin{pmatrix} F_{xT} & F_{yT} & M_T \end{pmatrix}^T$ will be used. The task of obtaining the individual braking forces from given virtual controls is performed by the control allocator, described in the following chapter.

Many previous approaches to rollover prevention are based on prevention of wheel lift-off [Johansson and Gäfvert, 2004]. While this is sufficient to prevent rollover, it may not be necessary, since roll stability may be maintained even after the loss of contact of a wheel. This approach may lead to conservative controllers which restrict maneuvering performance more than necessary. This is clearly undesirable in situations where extreme maneuvering is required to avoid an obstacle.

The strategy for roll control adopted here is to define a maximum allowable roll angle ϕ_{max} and design a controller to ensure that this limit is never exceeded. The choice of ϕ_{max} could come from an analysis of the dynamics of rollover such as that presented in the previous chapter, or could be chosen via experiments. Once a value of ϕ_{max} is decided, a corresponding limit on the total lateral force F_{yT} may be determined. From the friction ellipse, it can be seen that F_{yT} can be influenced by varying the total longitudinal (braking) force F_{xT}. The choice of F_{xT} constitutes the first part of the control design task. Yaw motion must then be controlled via the total moment M_T.

4.3 Roll Control

A bound on the roll angle may be translated into a bound on F_{yT} in the following way. From (2.25), the roll dynamics can be described by:

$$I_{xx}\ddot{\phi} + (C_\phi - mgh + (I_{zz} - I_{yy})\dot{\psi}^2)\phi + K_\phi\dot{\phi} = F_{yT}h$$

for small values of the roll angle ϕ. For reasonable values of the yaw rate $\dot{\psi}$ and the moments of inertia I_{zz} and I_{yy} the term $(I_{zz} - I_{yy})\dot{\psi}^2$ is much smaller than the term $C_\phi - mgh$ and may be neglected. The physical interpretation of this approximation is that the contribution to the roll angle of the motion of the vehicle about the z axis is much smaller than that of the rotation around the centre of curvature of the trajectory.

When this approximation is made, a scalar linear system is obtained. The transfer function from lateral force F_{yT} to roll angle ϕ is given by:

$$G_{roll}(s) = \frac{h}{I_{xx}s^2 + K_\phi s + C_\phi - mgh} \tag{4.1}$$

with corresponding impulse response $g_{roll}(t)$. The roll angle ϕ is given by:

$$\phi(t) = \int_0^\infty F_{yT}(t-\tau)g_{roll}(\tau)d\tau \tag{4.2}$$

$$\leq ||F_{yT}|| \underbrace{\int_0^\infty |g_{roll}(\tau)|d\tau}_{||G_{roll}||_{L_1}} \tag{4.3}$$

If the maximum allowable roll angle is given by ϕ_{max}, then the following inequality is obtained:

$$||F_{yT}|| \leq \frac{\phi_{max}}{||G_{roll}||_{L_1}} \tag{4.4}$$

This may be regarded as a dynamic lateral acceleration limit for a given maximum roll angle. Depending on the choice of ϕ_{max}, this relation will

give a lower limit for the lateral acceleration (or lateral force) than the static limits obtained in the previous chapter, which ignore the suspension dynamics.

Recalling the idea of the friction ellipse, it is possible to limit F_{yT} by choosing F_{xT} sufficiently large. By considering a friction ellipse for the entire vehicle, and ignoring the effects of steering, the following approximate relation is obtained:

$$F_{xT} \approx F_{xT,max}\sqrt{1-\left(\frac{F_{yT}}{F_{yT,max}}\right)^2} \tag{4.5}$$

where $F_{xT,max}$ and $F_{yT,max}$ are the maximum attainable generalized forces. Substituting the condition (4.4) into (4.5) gives:

$$|F_{xT}| \geq F_{xT,max}\sqrt{1-\left(\frac{\phi_{max}}{F_{yT,max}||G_{roll}||_{L_1}}\right)^2} \tag{4.6}$$

Proportional Control with Threshold-based Switching

A proportional controller may now be dimensioned using (4.6) which ensures that the maximum allowable lateral force is never exceeded. It should be noted that some tuning may be required if the bound (4.4) is too conservative. The total lateral force itself cannot be used for feedback as it is not measurable, but the lateral acceleration is measured and may be used. Assuming the sensor is positioned at the origin of the vehicle coordinate system, the lateral force is given by $F_{yT} = ma_y$. The total longitudinal force F_{xT} is regarded as the virtual control signal, and the control law is given by:

$$F_{xT} = -K_x m|a_y| \tag{4.7}$$

The gain K_x can be chosen so that the maximum allowable lateral force results in a control action satisfying (4.6). The control law may be combined with one of switching strategies presented in the previous chapter. As the control law is based on the lateral acceleration, it is natural to choose a switching method based on the same variable. The simplest algorithm is given by (3.10). A smoothing function is required

to provide smooth transitions between on and off modes. Using this strategy, the control law becomes:

$$F_{xT} = \begin{cases} -K_x \Upsilon m |a_y| & |a_y| \geq a_{y,threshold} \\ 0 & |a_y| < a_{y,threshold} \end{cases} \tag{4.8}$$

where Υ is a suitable smoothing function.

Constant Control with Dynamic Switching

An alternative strategy, similar to that proposed in [Odenthal *et al.*, 1999], is to use a constant value for F_{xT}, which satisfies (4.6). This could for example be combined with the PD-type switching strategy (3.13). To prevent chattering, hysteresis may be used. The resulting control law could take the form:

$$F_{xT} = \begin{cases} -m|a_x^d| & \text{if controller on} \\ 0 & \text{if controller off} \end{cases} \tag{4.9}$$

where a_x^d is the desired longitudinal acceleration. The controller is switched on when $\hat{a}_y \geq \hat{a}_y^{on}$ and off when $\hat{a}_y \leq \hat{a}_y^{off}$, where $\hat{a}_y^{on} > \hat{a}_y^{off}$ are predefined thresholds.

4.4 Yaw Control

Attention may now be directed at controlling the yaw rate a$\dot{\psi}$. From (2.23), it can be seen that the yaw rate can be influenced by both the total moment M_T and the total longitudinal force F_{xT}. Since the desired value of F_{xT} is given by the roll controller derived in the previous section, this can be assumed fixed, and M_T can be seen as the control variable for the yaw dynamics.

The purpose of the controller is to track a yaw rate reference signal, denoted $\dot{\psi}_{ref}$. The generation of this reference will be discussed later in the chapter. Since the yaw dynamics are nonlinear, it is appropriate to use a nonlinear control design methodology. A powerful tool often used in nonlinear control design is Lyapunov stability theory.

Lyapunov Theory

Lyapunov stability theory is a commonly used tool for analysis of nonlinear systems, as well as for the design of controllers. The theory allows the stability of particular solutions of a nonlinear system to be analyzed without solving the differential equations. In this section the main ideas of Lyapunov stability theory will be briefly presented. The reader is referred to [Slotine and Li, 1991] for an introduction to Lyapunov theory, and to [Khalil, 2002] for a more detailed treatment. The use of Lyapunov theory for control design is presented in [Kristić *et al.*, 1995].

Autonomous Systems Consider the system:

$$\dot{x} = f(x) \tag{4.10}$$

Assume without loss of generality that the system has an equilibrium point at $x = 0$.

DEFINITION 4.1
The equilibrium point $x = 0$ of (4.10) is:

- stable, if for each $\epsilon > 0$ there exists $\delta = \delta(\epsilon) > 0$ such that:

$$||x(0)|| < \delta \implies ||x(t)|| < \epsilon, \quad \forall t \geq 0$$

- unstable if not stable
- asymptotically stable if it is stable and δ can be chosen such that:

$$||x(0)|| < \delta \implies \lim_{t \to \infty} x(t) = 0$$

□

Lyapunov's method relies on the analysis of the properties of a scalar function $V(x)$, known as a Lyapunov function, to determine the properties of the solution of the system. This is commonly referred to as Lyapunov's direct method, or second method, and is summarised by the following theorem.

THEOREM 4.1
Let $x = 0$ be an equilibrium point of (4.10). Let $V : R^n \to R$ be a continuously differentiable function such that:

- $V(0) = 0$
- $V(x) > 0, \quad \forall x \neq 0$
- $||x(0)|| \to \infty \implies V(x) \to \infty$
- $\dot{V}(x) < 0, \quad \forall x \neq 0$

then $x = 0$ is globally asymptotically stable.
Proof:
For a proof see [Khalil, 2002, ch. 4]. □

Theorem 4.1 applies to autonomous systems. For the case of nonautonomous systems, this cannot be used directly, but corresponding theorems exist.

Nonautonomous Systems Consider the nonautonomous system:

$$\dot{x} = f(t, x) \tag{4.11}$$

The system has an equilibrium point at $x = 0$ at time $t = 0$ if:

$$f(t, 0) = 0, \quad \forall t \geq 0$$

DEFINITION 4.2
The equilibrium point $x = 0$ of (4.11) is:

- stable, if for each $\epsilon > 0$ there exists $\delta = \delta(\epsilon, t_0) > 0$ such that:

$$||x(t_0)|| < \delta \implies ||x(t)|| < \epsilon, \quad \forall t \geq t_0 \geq 0 \tag{4.12}$$

- uniformly stable if, for each $\epsilon > 0$ there exists $\delta = \delta(\epsilon) > 0$ independent of t_0 such that (4.12) is satisfied
- unstable if not stable
- asymptotically stable if it is stable and there exists a positive constant $c = c(t_0)$ such that $x(t) \to 0$ as $t \to \infty$ for all $||x(t_0)|| < c$

- uniformly asymptotically stable if it is uniformly stable and there exists a positive constant c, independent of t_0, such that for all $||x(t_0)|| < c$, $x(t) \to 0$ as $t \to \infty$ uniformly in t_0; that is, for each $\eta > 0$, there exists a $T = T(\eta) > 0$ such that:

$$||x(t)|| < \eta, \quad \forall t \geq t_0 + T(\eta), \ \forall ||x(t_0)|| < c$$

□

THEOREM 4.2
Let $x = 0$ be an equilibrium point for (4.11) and $D \subset R^n$ be a domain containing $x = 0$. Let $V : [0, \infty) \times D \to R$ be a continuously differentiable function such that:

$$W_1(x) \leq V(t,x) \leq W_2(x) \tag{4.13}$$

$$\frac{\partial V}{\partial t} + \frac{\partial V}{\partial x} f(t,x) \leq 0 \tag{4.14}$$

$\forall t \geq 0$ and $\forall x \in D$, where $W_1(x)$ and $W_2(x)$ are continuous positive definite functions on D. Then $x = 0$ is uniformly stable. If the inequality (4.14) is strengthened to:

$$\frac{\partial V}{\partial t} + \frac{\partial V}{\partial x} f(t,x) \leq -W_3(x) \tag{4.15}$$

where $W_3(x)$ is a continuous positive definite function on D, then $x = 0$ is uniformly asymptotically stable.
Proof:
For a proof see [Khalil, 2002, ch. 4]. □

An important condition in Theorem 4.2 is that the Lyapunov function $V(t,x)$ must be *decrescent*, that is, it must be upper bounded by some function $W_2(x)$.

Lyapunov-based Design for Yaw Rate Control

The task of the yaw rate controller is to track a given yaw rate reference trajectory $\dot{\psi}_{ref}$. The aim of the control design is therefore to render

$\dot{\psi} - \dot{\psi}_{ref} = 0$ a stable solution of the yaw dynamics. Since the yaw dynamics are given by a scalar system, a suitable Lyapunov function candidate is:

$$V = \frac{1}{2}(\dot{\psi} - \dot{\psi}_{ref})^2 \tag{4.16}$$

The yaw rate reference $\dot{\psi}_{ref} = \dot{\psi}_{ref}(t)$ is a function of time, so the Lyapunov function is time-dependent. The time derivative of V is given by:

$$\dot{V} = \frac{\partial V}{\partial t} + \frac{\partial V}{\partial \dot{\psi}} \frac{d\dot{\psi}}{dt} \tag{4.17}$$

$$= -(\dot{\psi} - \dot{\psi}_{ref}) \frac{d\dot{\psi}_{ref}}{dt} + (\dot{\psi} - \dot{\psi}_{ref}) \frac{d\dot{\psi}}{dt} \tag{4.18}$$

Introducing the yaw dynamics from (2.23) gives:

$$\dot{V} = (\dot{\psi} - \dot{\psi}_{ref}) \left(\frac{M_T - F_{xT} h \sin\phi - 2\dot{\phi}\dot{\psi}(I_{yy} - I_{zz}) \sin\phi \cos\phi}{I_{yy} \sin^2\phi + I_{zz} \cos^2\phi} - \right) - (\dot{\psi} - \dot{\psi}_{ref}) \ddot{\psi}_{ref} \tag{4.19}$$

The virtual controls F_{xT} and M_T may now be chosen such that the Lyapunov derivative becomes:

$$\dot{V} = -K_r(\dot{\psi} - \dot{\psi}_{ref})^2 \tag{4.20}$$

where K_r is a positive constant. By Theorem 4.2, the equilibrium $\dot{\psi} = \dot{\psi}_{ref}$ will then be uniformly asymptotically stable. Since F_{xT} is given by the roll control law (4.8), M_T can be found from:

$$M_T = (-K_r(\dot{\psi} - \dot{\psi}_{ref}) + \ddot{\psi}_{ref})(I_{yy} \sin^2\phi + I_{zz} \cos^2\phi) + F_{xT} h \sin\phi + 2\dot{\phi}\dot{\psi}(I_{yy} - I_{zz}) \sin\phi \cos\phi \tag{4.21}$$

Yaw Rate Reference Generation

A yaw rate reference $\dot{\psi}_{ref}$ is required for the yaw rate controller designed in the previous section. There are a number of ways of generating this. One approach is to use a simple vehicle model, such as a

linearized bicycle model as in (2.12). This approach is well suited to control applications used during steady state driving conditions, since the model is based on a number of approximations valid for small steering and slip angles. It is however of limited use in more extreme maneuvering.

Another simple approach, described in [Kiencke and Nielsen, 2000] is to define a maximum allowable yaw rate $\dot{\psi}_{max}$, and to obtain the yaw rate reference as:

$$\dot{\psi}_{ref} = \begin{cases} \dot{\psi} & |\dot{\psi}| \leq |\dot{\psi}_{max}| \\ \pm\dot{\psi}_{max} & |\dot{\psi}| > |\dot{\psi}_{max}| \end{cases}$$

This approach is appropriate for controlling yaw rate alone, since the controller is inactive when the yaw rate is within the allowed interval. However, it is less attractive in the context of the proposed control strategy, where the controller is switched on in order to prevent rollover. Another approach to reference generation is to calculate a desired radius of curvature, based on the current vehicle speed, and then to calculate a yaw rate reference based on this. Ignoring the effects of vehicle sideslip, the minimum achievable radius of curvature ρ_{min} is given by:

$$\rho_{min} = \frac{u^2}{a_{y,max}}$$

where u is the longitudinal velocity and $a_{y,max}$ is the maximum achievable (or allowed) lateral acceleration. The value of ρ_{min} can be calculated each time the controller is activated, and can then be used to generate a yaw rate reference:

$$\dot{\psi}_{ref} = \frac{u}{\rho_{min}} \tag{4.22}$$

This method of reference generation thus provides a yaw rate reference which corresponds to a minimum radius of curvature, and it therefore well suited to extreme maneuvers which may be caused by the need to avoid obstacles.

4.5 Summary

In this chapter, control design methodologies for obtaining the virtual control signals F_{xT} and M_T have been developed. These laws may be combined with the detection and switching methods presented in the previous chapter. In the following chapter, control allocation methods for conversion of these virtual controls into the actual control signals will be presented. Clearly, a large number of possible combinations of switching algorithms, control designs and control allocation methods exist. In the remainder of this thesis, the emphasis will be placed on those methods deemed most promising. In particular, the roll control strategy outlined in Section 4.3, along with the yaw rate control law (4.21) will be used. The resulting control law is outlined in Algorithm 4.1.

Algorithm 4.1: Control algorithm for generation of the virtual controls

Choose a_y^{on}, a_y^{off}, K_r, a_x^d ;
while *driving* **do**
  Filter a_y to obtain $\hat{a}_y$ using (3.13);
  if *controller off* & $\hat{a}_y \geq \hat{a}_y^{on}$ **then**
    controller on ;
    $u_{\text{start}} := u$;
    Calculate ρ_{ref} from u_{start};
    Calculate $\dot{\psi}_{ref}$ from ρ_{ref} ;
    Calculate $F_{xT} = -ma_x^d$;
    Calculate M_T from (4.21);
    else if *(controller on* & $\hat{a}_y \leq \hat{a}_y^{off}$*)* | *(controller off* & $\hat{a}_y < \hat{a}_y^{on}$*)* **then**
      controller off;
    else
      Calculate $\dot{\psi}_{ref}$ from ρ_{ref} ;
      Calculate $F_{xT} = -ma_x^d$;
      Calculate M_T from (4.21);
    end
  end
end

5

Control Allocation

5.1 Introduction

In the previous chapter, control design was carried out using generalized forces. These desired generalized forces must be converted to actual control signals in some way. This conversion is known as control allocation, and can be performed in a number of ways. In this chapter, control allocation based on convex optimization will be presented.

5.2 Problem Formulation

The role of the control allocator is to obtain *actual controls* which will give rise to the desired *virtual controls*. In general, the relationship is $v(t) = g(u(t))$ where $v(t) \in \mathbb{R}^k$ are the virtual controls, $u(t) \in \mathbb{R}^m$ are the actual controls and $g : \mathbb{R}^m \to \mathbb{R}^k$ is the mapping from actual to virtual controls, where $m > k$. The majority of the literature deals with the linear case [Härkegård, 2003], where the actual and virtual controls are related by a *control effectiveness matrix* B:

$$v(t) = Bu(t) \tag{5.1}$$

The control allocation problem is an under-determined, and often constrained problem. A wide variety of methods exist for solving allocation

problems, many of which are reviewed in [Härkegård, 2003]. A common approach is to formulate an optimization problem in which the magnitude of the allocation error:

$$\epsilon = ||Bu(t) - v(t)||_p, \quad p = 1, 2, \ldots$$

is minimized, subject to constraints and possibly additional costs on actuator use.

An important requirement imposed on the control allocation algorithm is that it must be implementable in a real-time environment. This is particularly important in automotive contexts, where sample times are typically of the order of 10ms. Algorithms with high levels of computational complexity are therefore not well suited to the application. Another requirement, particularly relevant to automotive applications, is that the number of sensors must be kept to a minimum. It is therefore desirable to use the minimum possible number of signals in control design.

5.3 Convex Optimization

In order to use optimization for control allocation, it is natural to construct convex optimization problems. Such problems posses many attractive properties, and efficient solvers exist for a wide range of problem formulations. Additionally, a very large number of problems can be posed as convex optimization problems. In this section, a number of different problem formulations will be outlined. In the following section, methods for solving these types of problems will be reviewed.

The general form of a convex optimization problem is:

$$\begin{aligned} &\text{minimize} && f_0(x) \\ &\text{subject to} && f_i(x) \leq b_i, \qquad i = 1, \ldots, m \end{aligned}$$

in which the objective function $f_0(x)$ and the constraints $f_i(x) \leq b_i$ are convex functions. The *feasible set* $\mathcal{P}$ of the optimization problem is the region in which the constraints are satisfied. The optimum x^* is the point in the feasible set where the objective function (also called cost function) is minimized. A number of sub–classes of convex problems exists, a number of which are outlined below.

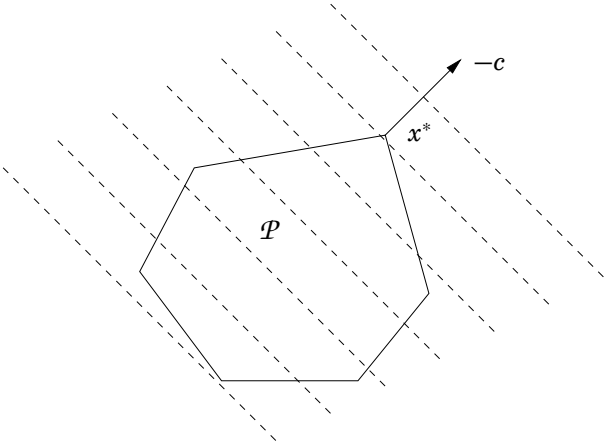

Figure 5.1 Interpretation of the solution of an LP problem, showing the active set $\mathcal{P}$ and the level curves of the objective function, which are hyperplanes orthogonal to c.

Linear Programs

Linear Programs (LP) are convex problems in which both the objective and constraint functions are affine. They have the form:

$$\begin{array}{ll} \text{minimize} & c^T x + d \\ \text{subject to} & Gx \leq h \\ & Ax = b \end{array}$$

The feasible set of an LP is a polyhedron, and since the objective function is linear, the level curves are given by hyperplanes orthogonal to c. The feasible set and level curves of a general LP are illustrated in Figure 5.1.

Quadratic Programs with Linear Constraints

In Quadratic Programs (QP), the objective function is convex quadratic.

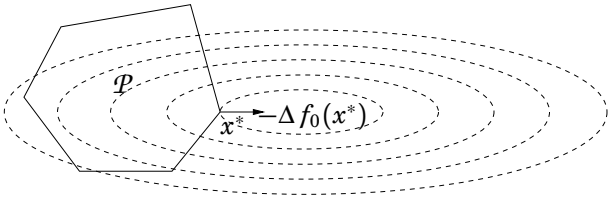

Figure 5.2 Interpretation of the solution of an QP problem, showing the active set $\mathcal{P}$ and the level curves of the objective function.

When linear constraints are present, the problem has the form:

$$\begin{aligned} \text{minimize} \quad & \frac{1}{2}x^T P x + q^T x + r \\ \text{subject to} \quad & Gx \leq h \\ & Ax = b \end{aligned}$$

Figure 5.2 gives a graphical interpretation of a linearly-constrained quadratic programming (LCQP) problem.

Quadratic Programs with Quadratic Constraints

Another class of QPs are those in which the both the objective function and the constraints are convex quadratic:

$$\begin{aligned} \text{minimize} \quad & \frac{1}{2}x^T P_0 x + q_0^T x + r_0 \\ \text{subject to} \quad & \frac{1}{2}x^T P_i x + q_i^T x + r_i \leq 0, \quad i = 1, \ldots, m \\ & Ax = b \end{aligned}$$

This type of problem is referred to as a quadratically-constrained quadratic programming (QCQP) problem.

5.4 Solving Convex Optimization Problems

Posing control allocation problems as convex optimization problems is attractive since there is a wide variety of efficient solvers for different

types of problems. Two classes of methods are of particular interest to the optimization problems considered in this chapter, *Interior Point* and *Active Set* methods.

Interior point methods can be used for convex problems that include inequality constraints, such as QCQP problems. A detailed presentation of interior point methods can be found in [Boyd and Vandenberghe, 2004].

Active set methods are based on finding the active constraints and solving simpler equality-constrained problems. These methods are particularly suitable for control allocation, for several reasons. Primarily, active set algorithms have the appealing property that a feasible solution is available after each iteration. For applications in a real-time environment this is particularly useful, since it means that if the algorithm must be interrupted, a feasible (albeit suboptimal) solution will always be available. In addition, active set methods become much more efficient when a good estimate of the active set is available. For control allocation purposes, a good estimate of the active set is usually given by the active set from the previous sample. In order to maximize efficiency, the structure of the problem must be utilized to select the most effective solver. Active set methods for control allocation are discussed in more detail in [Härkegård, 2003].

5.5 Control Allocator Design

The control laws derived in the previous chapter use the generalized forces F_{xT}, F_{yT} and M_T as virtual controls. The aim of the control allocator is to obtain actual control signals which give rise to the desired virtual controls, while respecting certain constraints. The actual control signals in this case are taken to be the longitudinal tire forces. In reality the control commands are the brake pressures, but a simple relationship exists between these quantities. In this section, two methodologies for control allocator design are presented. The first is based on [Johansson and Gäfvert, 2004], and the second is a new approach.

Method 1: Formulation of a QCQP Allocation Problem

In this approach, both the longitudinal and lateral tire forces F_{xi} and

F_{yi} are regarded as actual controls, with:

$$u = \begin{pmatrix} F_x^{fl} & F_x^{fr} & F_x^{rl} & F_x^{rr} & F_y^{fl} & F_y^{fr} & F_y^{rl} & F_y^{rr} \end{pmatrix}^T$$

Define the vector of virtual controls as:

$$v = \begin{pmatrix} F_{xT} \\ F_{yT} \\ M_T \end{pmatrix} \tag{5.2}$$

The virtual and actual controls are related by the control effectiveness matrix:

$$Bu = v$$

Control Effectiveness Matrix Derivation The control effectiveness matrix is then given by:

$$B^T = \begin{pmatrix} \cos\delta & \sin\delta & (a\sin\delta + l\cos\delta) \\ \cos\delta & \sin\delta & (a\sin\delta - l\cos\delta) \\ 1 & 0 & l \\ 1 & 0 & -l \\ -\sin\delta & \cos\delta & (a\cos\delta - l\sin\delta) \\ -\sin\delta & \cos\delta & (a\cos\delta + l\sin\delta) \\ 0 & 1 & -b \\ 0 & 1 & -b \end{pmatrix} \tag{5.3}$$

Constraints A number of constraints are present. The control signals are purely braking forces, giving rise to the constraint:

$$F_{xi} \leq 0 \tag{5.4}$$

The maximum allowable braking force is determined by the coefficient of friction μ between the tire and the road, as well as the vertical wheel load F_z, which can be expressed as:

$$F_{xi} \geq -|\mu F_{zi}| \tag{5.5}$$

The lateral force must act in the correct direction (the same direction as the maximum force $F_{yi,max}$). This can be expressed as:

$$F_{yi}F_{yi,max} \geq 0 \tag{5.6}$$

Finally, there are the constraints arising from the friction ellipse:

$$\left(\frac{F_y}{F_{y,max}}\right)^2 + \left(\frac{F_x}{F_{x,max}}\right)^2 \leq 1 \tag{5.7}$$

These constraints can be expressed as norm constraints, on the form:

$$||W_i u|| \leq 1 \tag{5.8}$$

where the matrices W_i have the form:

$$W_{FL} = \begin{pmatrix} \frac{1}{F_{yFL,max}} & 0 & 0 & 0 & 0 & 0 & 0 & 0 \\ 0 & 0 & 0 & 0 & 0 & 0 & 0 & 0 \\ 0 & 0 & 0 & 0 & 0 & 0 & 0 & 0 \\ 0 & 0 & 0 & 0 & 0 & 0 & 0 & 0 \\ 0 & 0 & 0 & 0 & \frac{1}{\mu F_{zFL}} & 0 & 0 & 0 \\ 0 & 0 & 0 & 0 & 0 & 0 & 0 & 0 \\ 0 & 0 & 0 & 0 & 0 & 0 & 0 & 0 \\ 0 & 0 & 0 & 0 & 0 & 0 & 0 & 0 \end{pmatrix} \tag{5.9}$$

If a convex optimization problem is posed using the equality constraint (5.1), the presence of the other constraints may make the problem infeasible (no solution exists which satisfies all the constraints). To avoid this, a slack variable γ is introduced. Replacing the equality constraint (5.1) with the inequality:

$$||Bu - v|| \leq \gamma \tag{5.10}$$

allows the optimization problem can be written as:

$$\begin{aligned} \text{minimize} \quad & \gamma \\ \text{subject to} \quad & ||Bu - v|| \leq \gamma \\ & ||W_i u|| \leq 1 \\ & F_{yi} F_{yi,max} \geq 0 \\ & F_{xi} \leq 0 \\ & F_{xi} \geq -|\mu F_{zi}| \end{aligned} \tag{5.11}$$

This is a quadratically-constrained quadratic program (QCQP). This particular case of a linear objective function together with quadratic inequality constraints is known as a second order cone programming (SOCP) problem. Second order cone problems may be solved using interior point methods.

Method 2: Formulation of a LCQP Allocation Problem

The second order cone problem posed in (5.11) can be solved efficiently with interior point methods, but it is unlikely that the solution can be found sufficiently quickly to allow real-time implementation. It is clear that some simplification of the problem may be advantageous. Regarding the computational complexity of the algorithm, a key issue is the type of constraints present. The constraints derived from the friction ellipse are quadratic, which increases the complexity of the problem and requires greater computation time for calculating the solution. In addition, the sideslip angles of the wheels α_i and the normal tire forces F_{zi} must be known in order to calculate the values of $F_{yi,max}$ used in the constraints in (5.11). This represents additional information which must be either measured or estimated. It is therefore proposed to make approximations which both simplify the constraints and reduce the amount of extra information required.

Since the controller will be operating exclusively in the limits of the vehicle's driving regime, it is reasonable to make approximations which are valid during these conditions. The first approximation is that the slip angles of all of the wheels are large enough such that the maximum lateral tire forces saturate, and are thus given by $F_{yi,max} = \mu F_{zi}$. This is attractive since the slip angles are no longer required in order to compute the maximum lateral forces. The resultant force on each

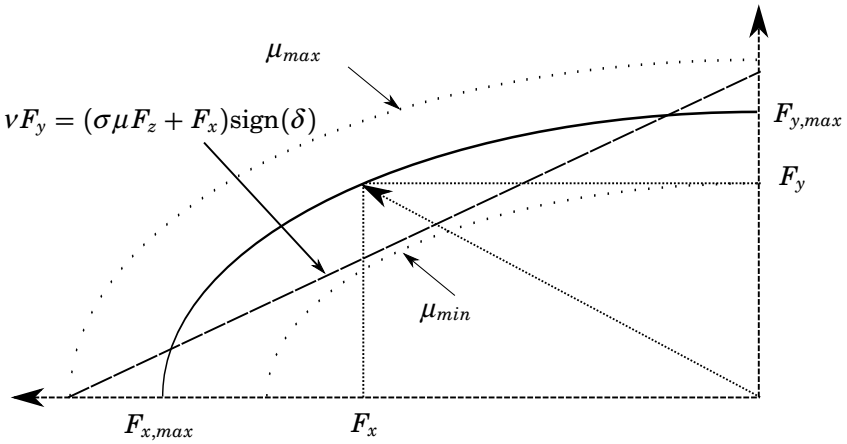

Figure 5.3 The friction ellipse with linear approximation, showing the uncertainty regions arising from the uncertainty of μ. Note that the linear approximation is only valid for $-\sigma\mu F_z \leq F_x \leq 0$. The approximation must therefore be used with constraints to obtain reasonable results.

wheel can now be seen as a function of the applied braking force and the normal force. However, the function is still nonlinear (the friction ellipse becomes a circle when $F_{yi,max} = F_{xi,max}$), so a further approximation is suggested to simplify the constraints. The friction ellipse can be approximated in each quadrant by a linear function, as in Figure 5.3. This approximation can be justified by considering that there will be a large amount of uncertainty in the radius of the friction circle. In particular, μ is highly uncertain. The linear approximation can be thought of as lying within circles defined by upper and lower bounds of the radius μF_z. The approximation may be refined by introducing tuning parameters to alter the gradient and position of the linear approximations, giving a relationship on the form:

$$\nu F_y = (\sigma\mu F_z + F_x)\text{sign}(\delta) \tag{5.12}$$

The sign(δ) factor is required to ensure that the resultant force acts in the correct direction. This approximation has the attractive property that the constraints are convex. In the formulation (5.11), it is assumed that the resultant force lies within the ellipse, rather than on

the boundary, in order to obtain convex constraints. Using these simplifications, a new control allocation problem can now be formulated.

Replacing F_y with the linear approximation (5.12), and defining $\Delta = \text{sign}(\delta)$, the relationships between braking forces and the generalized forces become:

$$\begin{aligned} F_{xT} =&(\cos\delta - \frac{\Delta}{\nu}\sin\delta)(F_x^{fl} + F_x^{fr}) - \frac{\sigma\mu\Delta\sin\delta}{\nu}(F_z^{fl} + F_z^{fr}) \\ &+ F_x^{rl} + F_x^{rr} \end{aligned} \tag{5.13}$$

$$\begin{aligned} F_{yT} =&(\frac{\Delta}{\nu}\cos\delta + \sin\delta)(F_x^{fl} + F_x^{fr}) + \sigma\mu\Delta(F_x^{rl} + F_x^{rr}) \\ &+ \frac{\sigma\mu\Delta\cos\delta}{\nu}(F_z^{fl} + F_z^{fr}) + \frac{\sigma\mu\Delta}{\nu}(F_z^{rl} + F_z^{rr}) \end{aligned} \tag{5.14}$$

$$\begin{aligned} M_T =&(\frac{\Delta}{\nu}(a\cos\delta + l\sin\delta) + a\sin\delta - l\cos\delta)F_x^{fl} \\ &+ (\frac{\Delta}{\nu}(a\cos\delta - l\sin\delta) + a\sin\delta + l\cos\delta)F_x^{fr} \\ &+ \frac{\sigma\mu\Delta}{\nu}(a\cos\delta + l\sin\delta)F_z^{fl} + \frac{\sigma\mu\Delta}{\nu}(a\cos\delta - l\sin\delta)F_z^{fr} \\ &+ F_x^{rl}(-l - b\frac{\Delta}{\nu}) + F_x^{rr}(l - b\frac{\Delta}{\nu}) - \frac{b\sigma\mu\Delta}{\nu}(F_z^{rl} + F_z^{rr}) \end{aligned} \tag{5.15}$$

This may be written in vector form as:

$$\begin{aligned} F_{xT} =&\begin{pmatrix} (\cos\delta - \frac{\Delta}{\nu}\sin\delta) & (\cos\delta - \frac{\Delta}{\nu}\sin\delta) & 1 & 1 \end{pmatrix} u \\ &- \frac{\sigma\mu\Delta\sin\delta}{\nu}(F_z^{fl} + F_z^{fr}) \end{aligned} \tag{5.16}$$

$$\begin{aligned} F_{yT} =&\begin{pmatrix} (\frac{\Delta}{\nu}\cos\delta + \sin\delta) & (\frac{\Delta}{\nu}\cos\delta + \sin\delta) & \frac{\Delta}{\nu} & \frac{\Delta}{\nu} \end{pmatrix} u \\ &+ \frac{\sigma\mu\Delta\cos\delta}{\nu}(F_z^{fl} + F_z^{fr}) + \frac{\sigma\mu\Delta}{\nu}(F_z^{rl} + F_z^{rr}) \end{aligned} \tag{5.17}$$

$$\begin{aligned} M_T =&\begin{pmatrix} b_M^1 & b_M^2 & (-l - b\frac{\Delta}{\nu}) & (l - b\frac{\Delta}{\nu}) \end{pmatrix} u \\ &+ \frac{\sigma\mu\Delta}{\nu}\left(a\cos\delta(F_z^{fl} + F_z^{fr}) + l\sin\delta(F_z^{fl} - F_z^{fr}) - b(F_z^{rl} + F_z^{rr})\right) \end{aligned} \tag{5.18}$$

with $u = \begin{pmatrix} F_x^{fl} & F_x^{fr} & F_x^{rl} & F_x^{rr} \end{pmatrix}^T$, and where:

$$b_M^1 = (\frac{\Delta}{\nu}(a\cos\delta + l\sin\delta) + a\sin\delta - l\cos\delta)$$
$$b_M^2 = (\frac{\Delta}{\nu}(a\cos\delta - l\sin\delta) + a\sin\delta + l\cos\delta)$$

The virtual controls v can now be expressed as:

$$v = \underbrace{\begin{pmatrix} (\cos\delta - \frac{\Delta}{\nu}\sin\delta) & (\cos\delta - \frac{\Delta}{\nu}\sin\delta) & 1 & 1 \\ (\frac{\Delta}{\nu}\cos\delta + \sin\delta) & (\frac{\Delta}{\nu}\cos\delta + \sin\delta) & \frac{\Delta}{\nu} & \frac{\Delta}{\nu} \\ b_M^1 & b_M^2 & (-l - b\frac{\Delta}{\nu}) & (l - b\frac{\Delta}{\nu}) \end{pmatrix}}_{B} u + \underbrace{\begin{pmatrix} -\frac{\sigma\mu\Delta\sin\delta}{\nu}(F_z^{fl} + F_z^{fr}) \\ \frac{\sigma\mu\Delta\cos\delta}{\nu}(F_z^{fl} + F_z^{fr}) + \frac{\sigma\mu\Delta}{\nu}(F_z^{rl} + F_z^{rr}) \\ \frac{\sigma\mu\Delta}{\nu}\left(a\cos\delta(F_z^{fl} + F_z^{fr}) + l\sin\delta(F_z^{fl} - F_z^{fr}) - b(F_z^{rl} + F_z^{rr})\right) \end{pmatrix}}_{d}$$

This gives the desired linear relationship between actual and virtual controls:

$$v(t) = Bu(t) + d \tag{5.19}$$

This can be transformed into the required form in (5.1) by defining new virtual controls $v'(t) = v(t) - d$. The vector d depends only on the normal forces F_{zi}, and is constant at each sample time. The constraints are now given by:

$$-|\sigma\mu F_{zi}| \leq F_{xi} \leq 0 \tag{5.20}$$

These constraints have the form of 'box constraints':

$$\underline{u} \leq u \leq \overline{u} \tag{5.21}$$

This type of constraint allows the formulation of an optimization problem with a special structure, which allows rapid computation.

Optimization Problem A linearly-constrained quadratic programming problem may be formulated. Such problems may take the form:

$$\begin{aligned} u &= \arg\min_{u\in\Omega} ||W_u(u-u_d)||_2 \\ \Omega &= \arg\min_{\underline{u}\le u\le\overline{u}} ||W_v(Bu-v')||_2 \end{aligned} \tag{5.22}$$

where W_u and W_u are diagonal weighting matrices, u_d is a desired actual control value, and $\underline{u}$ and $\overline{u}$ are constraints on the actual controls. This type of problem is known as Sequential Least-Squares (SLS), since the solution is computed in two steps. First, the weighted allocation error $||W_v(Bu-v')||$ is minimized. If feasible solutions are found, then the 'best' solution is obtained by minimizing $||W_u(u-u_d)||$.

A faster algorithm can be obtained by approximating the SLS formulation as a Weighted Least-Squares (WLS) problem:

$$u = \arg\min_{\underline{u}\le u\le\overline{u}} \left(||W_u(u-u_d)||_2^2 + \gamma||W_v(Bu-v')||_2^2\right) \tag{5.23}$$

Here, the solution is calculated in a single step. The parameter γ is typically chosen to be very large in order to emphasize the importance of minimizing the allocation error.

Calculating the Solution Active set methods for the solution of the optimization problems (5.22) and (5.23) are presented in [Härkegård, 2003]. These methods will be briefly reviewed here.

Consider the least squares problem:

$$\min_u ||Au-b|| \tag{5.24a}$$

$$Bu = v \tag{5.24b}$$

$$\underbrace{\begin{pmatrix} I \\ -I \end{pmatrix}}_{C} u \ge \underbrace{\begin{pmatrix} \underline{u} \\ -\overline{u} \end{pmatrix}}_{U} \tag{5.24c}$$

The principal idea of active set methods is that in each step, some of the inequality constraints are taken to be equality constraints, while the remainder are ignored. Denote with $\mathcal{W}$ the *working set*, which

Algorithm 5.1: Active set algorithm

Let u^0 be a feasible starting point, satisfying (5.24c) ;
for $i = 0, 1, 2, \ldots$ **do**
Given suboptimal iterate u^i, find the optimal perturbation p, considering the inequality constraints in $\mathcal{W}$ as equality constraints and ignoring the remainder. This is done by solving:

$$\begin{aligned} \min_p & ||A(u^i + p) - b|| \\ & Bp = 0 \\ & p_i = 0, \quad i \in \mathcal{W} \end{aligned}$$

if $u^i + p$ *feasible* **then**
Set $u^{i+1} = u^i + p$;
Compute Lagrange multipliers as:

$$A^T(Au - b) = \begin{pmatrix} B^T & C_0^T \end{pmatrix} \begin{pmatrix} \mu \\ \lambda \end{pmatrix}$$

where C_0 consists of the rows of C corresponding to the constraints in the active set ;
if $\lambda \geq 0$ **then**
u^{i+1} is optimal solution;
Return $u = u^{i+1}$
else
Remove constraint corresponding to most negative λ from the working set $\mathcal{W}$;
end

contains all of the active constraints. Algorithm 5.1 outlines an active set method for finding the solution of the least squares problem above.

The weighted least squares problem may now be solved using Algorithm 5.2.

Algorithm 5.2: Solution of the WLS control allocation problem (5.23)

Obtain the initial working set $\mathcal{W}$ from the active set from the previous sampling interval ;
Obtain the starting point u^0 from the optimal point from the previous sampling interval ;
Rewrite the cost function as:

$$||W_u(u-u_d)||_2^2 + \gamma||W_v(Bu-v')||_2^2 = \left\| \underbrace{\begin{pmatrix} \gamma^{\frac{1}{2}} W_v B \\ W_u \end{pmatrix}}_{A} u - \underbrace{\begin{pmatrix} \gamma^{\frac{1}{2}} W_v v \\ W_u u_d \end{pmatrix}}_{b} \right\|^2$$

Use Algorithm 5.1 to solve:

$$u = \arg\min_u ||Au-b||$$
$$\underline{u} \le u \le \overline{u}$$

Parameter Selection Since only F_{xT} and M_T are used as virtual controls, F_{yT} may effectively be removed from the allocation problem by making the corresponding weight in the matrix W_v small relative to the other weights. The relative magnitudes of the remaining weights can be used to determine which virtual control is given priority, in cases where both cannot be satisfied simultaneously. For example, F_{xT} is the most critical virtual control for prevention of rollover, so the corresponding entry in W_v can be chosen to be larger than the others.

The desired actual control vector u_d can be chosen in a number of ways. One possibility is to choose it as the actuator position that would be obtained in the absence of constraints:

$$u_d = B^\dagger v'$$

where $B^\dagger$ is the pseudo-inverse of B.

The weighting matrix W_u can be used to influence the distribution of the control actions among the actuators. It is most useful in cases

where different types of actuators are present and preference should be given to a particular type. In this thesis the actuators are all of the same type so the choice of W_u is not critical.

Rate Constraints

Rate constraints in the actuators (in this case the braking system) may be taken into account in the control allocation problem by modifying the constraints at each sample time. Let the rate constraints be given by:

$$r_{min} \leq \dot{u}(t) \leq r_{max} \tag{5.25}$$

Approximating the derivative with the backward difference method:

$$\dot{u}(t) \approx \frac{u(t) - u(t - T_s)}{T_s}$$

where T_s is the sampling period allows the rate constraints to be rewritten as position constraints. The maximum allowable deviations of the positions from one sample time to another are given by:

$$\Delta_{min} = r_{min} T_s$$
$$\Delta_{max} = r_{max} T_s$$

The new constraints are given by:

$$\underline{u}^*(t) = \max\{\underline{u}, u(t - Ts) + \Delta_{min}\} \tag{5.26}$$
$$\overline{u}^*(t) = \min\{\overline{u}, u(t - Ts) + \Delta_{max}\} \tag{5.27}$$

The rate constraints present in the control problem are the brake pressure rising and falling slew rates. These are summarized in Table 5.1. Since the braking forces are negative, the maximum rising slew rate corresponds to the minimum rate of change r_{min}, and the maximum falling slew rate corresponds to r_{max}. The brake pressure slew rates are converted into force rates of change using the appropriate scaling factors.

Max. rising slew rate	200 bar/s
Max. falling slew rate	1000 bar/s

Table 5.1 Brake pressure rate constraints

Warmstarting

The active set algorithm provides both the solution to the QP problem, as well as the current active set. The active set is the set of constraints which are currently active for the given solution. In control allocation, where the QP problem is solved at each sample time, it is very common that the active set obtained at a given sample time will also be the optimal active set at the next sample time. This implies that the previous active set and optimum point found in one sample time may be used as the starting point for the optimization problem in the following sample time, thereby reducing the number of iterations required to find the new solution. The use of the previous sample's solution and active set as the starting point for the next optimization is sometimes called 'warmstarting', and may significantly reduce the average computation time required to solve the control allocation problem.

The use of the previous optimum and active set is included in Algorithm 5.2. However, problems can occur in the case of time varying constraints. In the control allocation problem presented here, the constraints depend on the normal forces F_{zi}, which are time dependent. Time variations of the constraints also occur when rate constraints are incorporated. This time variation presents two problems:

- The previously calculated optimum $u(t-1)$ may no longer be feasible at time t and can thus no longer be used as a starting point for the algorithm
- Elements of the optimum $u(t-1)$ that were saturated (meaning that their corresponding constraints were active) may no longer be saturated at time t. The active set at time $t-1$ may therefore no longer be valid at time t and may require updating.

To avoid these problems, the algorithm for the solution of the WLS problem may be modified to include a feasibility check for the starting point of the algorithm as well as updating of the active set. Algorithm

5.3 includes these modifications.

Algorithm 5.3: Solution of the WLS control allocation problem (5.23)

Let u^0 be the optimal point obtained at time $t-1$, and $\mathcal{W}^0$ be the corresponding active set ;
if $\underline{u}(t) < u^0 < \overline{u}(t)$ **then**
    Remove any active constraints from $\mathcal{W}^0$;
else
    Saturate the infeasible elements of u^0 and update the initial working set $\mathcal{W}^0$;
Rewrite the cost function as:

$$||W_u(u-u_d)||_2^2 + \gamma||W_v(Bu-v')||_2^2 = \left\| \underbrace{\begin{pmatrix} \gamma^{\frac{1}{2}} W_v B \\ W_u \end{pmatrix}}_{A} u - \underbrace{\begin{pmatrix} \gamma^{\frac{1}{2}} W_v v \\ W_u u_d \end{pmatrix}}_{b} \right\|^2$$

Use Algorithm 5.1 to solve:

$$u = \arg\min_u ||Au-b||$$
$$\underline{u} \le u \le \overline{u}$$

Summary

The control allocation methods presented in this chapter are used to convert the virtual control signals into actuator inputs. By making appropriate approximations, a linearly constrained quadradic programming problem has been posed. The problem has a special structure which allows rapid solution. This is imperative since the algorithm must be used online.

An additional element present in the control loop is the Anti-lock Brake System (ABS). The ABS system is used to prevent wheel lock, and may alter the outputs of the control allocator when active. Control design for ABS is not considered in this thesis; the reader is referred to [Solyom, 2004; Johansson and Rantzer, 2003].

6

Results

6.1 Introduction

To fully evaluate the performance of any vehicle control algorithm, experiments with real vehicles are required. Initial design evaluations are however typically carried out with the help of simulations. Modern computing tools allow the use of very advanced vehicle simulations, which accurately reproduce the behaviour of actual vehicles. Testing via simulation is therefore an important step in the development of new algorithms. In this chapter, simulation results of the proposed strategies are presented.

Simulation Environment

The simulations presented in this chapter were carried out in Matlab/Simulink using DaimlerChrysler's CASCaDE (Computer Aided Simulation of Car, Driver and Environment) software. CASCaDE is an advanced vehicle simulator, incorporating accurate tire models and full degree-of-freedom chassis models. In addition to the vehicle dynamics, the simulator includes other control systems such as Anti-lock Braking Systems (ABS). This is extremely important since these subsystems affect the control system outputs, in this case the braking forces. The vehicle used in the simulations was a commercial van with a gross weight of roughly 3500kg. A number of test maneuvers were simulated. These will be described in the next section.

6.2 Test Maneuvers

Due to the dangerous nature of rollover accidents, a number of vehicle safety organisations have evaluated the performance of production vehicles to assess their safety. In order to obtain a common measure, a number of standardized maneuvers have been developed. The National Highway Traffic Safety Administration (NHTSA) has developed various standard maneuvers, including the so-called fishhook and J-turn maneuvers, which are described here.

Fishhook

The fishhook maneuver is an important test maneuver in the context of rollover. It attempts to maximize the roll angle under transient conditions and is performed as follows, with a start speed of 80km/h[1]:

- The steering wheel angle is increased at a rate of 720deg/sec up to $6.5\delta_{stat}$, where δ_{stat} is the steering angle which is necessary to achieve 0.3g stationary lateral acceleration at 80km/h
- This value is held for 250ms
- The steering wheel is turned in the opposite direction at a rate of 720 deg/sec until it reaches -$6.5\delta_{stat}$

Figure 6.1 illustrates the driver input during a Fishhook maneuver. No brake or accelerator commands are given during the maneuver.

J-Turn

The J-turn is a simple step in the steering wheel angle driving the vehicle towards the physical limits. This maneuver can cause a roll over of vehicles with critical load. The speed of the vehicle just before the step input to the steering wheel angle is 60 mph (approximately 96 km/h). After releasing the accelerator pedal the steering wheel angle is increased at a rate of 1000deg/sec until it reaches 8 times the value δ_{stat} (the steer angle which is necessary to achieve 0.3g stationary lateral acceleration at 50mph (approx. 80km/h) . The steering input for this maneuver is illustrated in Figure 6.2.

[1]The original specification from the NHTSA is given in imperial units and states a start speed of 50 mph. Metric conversions will be used in this thesis.

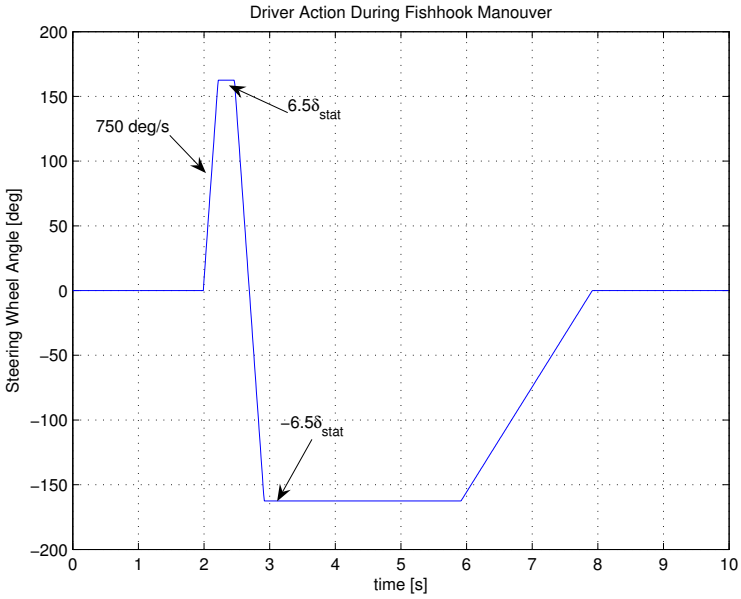

Figure 6.1 Driver input during the fishhook maneuver.

Roll Rate Feedback Fishhook

A modified version of the fishhook maneuver, known as the roll rate feedback fishhook maneuver, can also be specified. This maneuver is optimized for producing maximum vehicle roll. The sequence of events is similar to the standard fishhook, but the second steering angle change is performed only after the roll rate becomes small (that is, when the roll angle reaches its maximum). The maneuver is performed as follows, with a start speed of 80km/h:

- The steering wheel angle is increased at a rate of 720deg/sec up to 6.5 times δ_{stat}
- This value is held until the roll rate drops below 1.5 deg/sec
- The steering wheel is turned in the opposite direction at a rate of 720 deg/sec until it reaches -6.5δ_{stat}

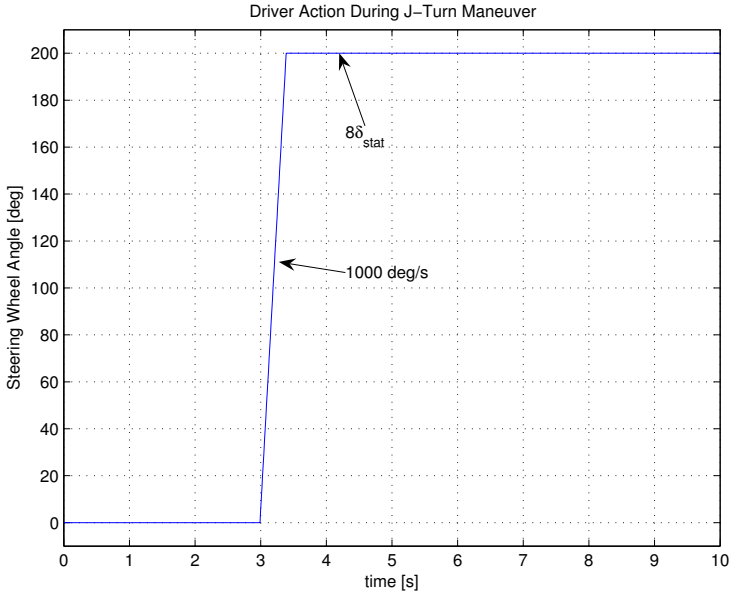

Figure 6.2 Driver input during the J-turn maneuver.

6.3 Simulation Results

In this section simulation results relating to the fishhook and J-turn maneuvers are presented. The control strategies were found to work well for a large number of different test maneuvers, but priority will be given here to the fishhook and J-turn, as they are standard maneuvers, specifically intended for the investigation of both roll and yaw stability.

The results presented here use the control strategy outlined in Algorithm 4.1, and the control allocation strategy in Algorithm 5.3. The control allocation problem was solved using the Quadratic Control Allocation Toolbox (QCAT) for Matlab written by Ola Härkegård, which contains implementations of the algorithms described in [Härkegård, 2003].

Fishhook Maneuver

The fishhook maneuver described in the previous section and illustrated in Figure 6.1 was the primary test maneuver used for evaluating and tuning the control strategies. The standard vehicle setup used in the simulations was a vehicle with an additional load of 420kg. The vehicle parameters used in the fishhook simulations are summarized in Table 6.1. The controller parameters used in all the simulations are summarized in Table 6.2

Controller Inactive Figure 6.3 shows the effect of the fishhook maneuver when the controller is inactive. Rollover occurs after approximately 4.5 seconds, just after the maximum value of the second steering action is attained. The severe instability of the roll dynamics can clearly be seen. The roll rate increases faster than linearly, which is consistent with the analysis in Chapter 3 which predicted increasingly unstable roll dynamics as the roll angle increases.

Controller Active Figure 6.4 shows the states of the vehicle when the controller is active. The roll angle limit used was 0.1 radians. It can be seen that this limit is not exceeded during the maneuver.

The yaw rate tracking is reasonable, although the reference is not followed exactly. One of the aims of performing yaw rate control is the limitation of the sideslip angle β. A maximum value of β can be defined as [Kiencke and Nielsen, 2000]:

$$\beta_{max} = 10^\circ - 7^\circ \frac{(u^2 + v^2)}{(40)^2}$$

This maximum value of the sideslip value is illustrated in Figure 6.4. It can be seen that β remains within the allowed range throughout the maneuver.

Control Allocation Figures 6.5, 6.6 and 6.7 show the desired virtual controls F_{xT}, M_T and F_{yT}, as well as the generalized forces that were obtained using the resulting braking actions. The 'predicted' or expected generalized forces are also shown. These are calculated in the control allocation algorithm and are given by:

$$v_o = Bu_o$$

where v_o are the expected generalized forces, u_o are the actual controls obtained by the control allocator and B is the control effectiveness matrix. It is interesting to examine these signals to ascertain whether model used in the control allocation algorithm is accurate.

It can be seen that both of the virtual control commands F_{xT} and M_T are met to a good degree of accuracy. In addition, the generalized forces calculated with the model used by the control allocation algorithm agree closely with the actual generalized forces that were obtained.

Constraints Figure 6.8 shows the forces acting on each of the tires. As expected, due to the load transfer the rear right tire loses contact with the road for a time during the simulation. Since the control strategy is based on limitation of the roll angle and not on prevention of wheel lift-off, this is acceptable behaviour.

Figure 6.9 illustrates the desired and actual brake pressures during the simulation. The importance of rate constraints in the control allocation algorithm can be seen by comparing Figure 6.9 with Figure 6.10, in which the rate constraints have been deactivated.

Switching Figure 6.11 shows the lateral acceleration during the simulation. Figure 6.12 shows both the lateral acceleration and the filtered version $\hat{a}_y$, given by (3.13), which is used for switching. It is clear that incorporating gradient information allows earlier switching, which gives improved performance.

Trajectory following The trajectories of the vehicle during the fishhook maneuver with and without control are shown in Figure 6.13. It can be seen that the vehicle follows the desired fishhook trajectory when the controller is active. A comparison of the entire trajectory between the controlled and uncontrolled vehicles is difficult since the uncontrolled vehicle rolls over during the maneuver. Under the assumption that the maneuver is performed for collision avoidance, it can be seen that the radii of curvature achieved by the controlled vehicle are comparable to or better than the uncontrolled vehicle.

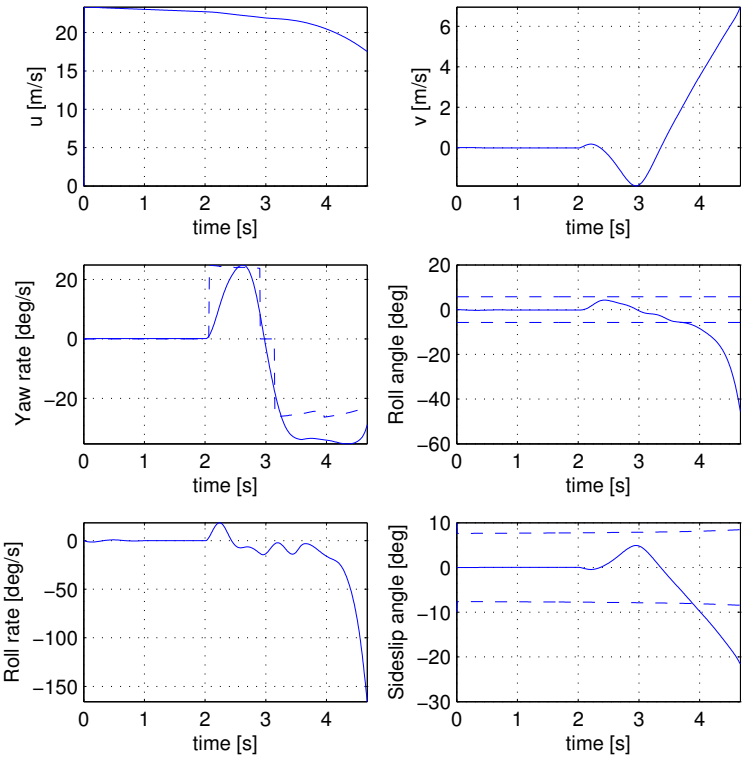

Figure 6.3 Vehicle states during the fishhook maneuver with the controller inactive. The severe instability of the roll dynamics is clearly visible. The rapid growth of both the roll angle and roll rate is evident. The simulation ceases to run after rollover occurs.

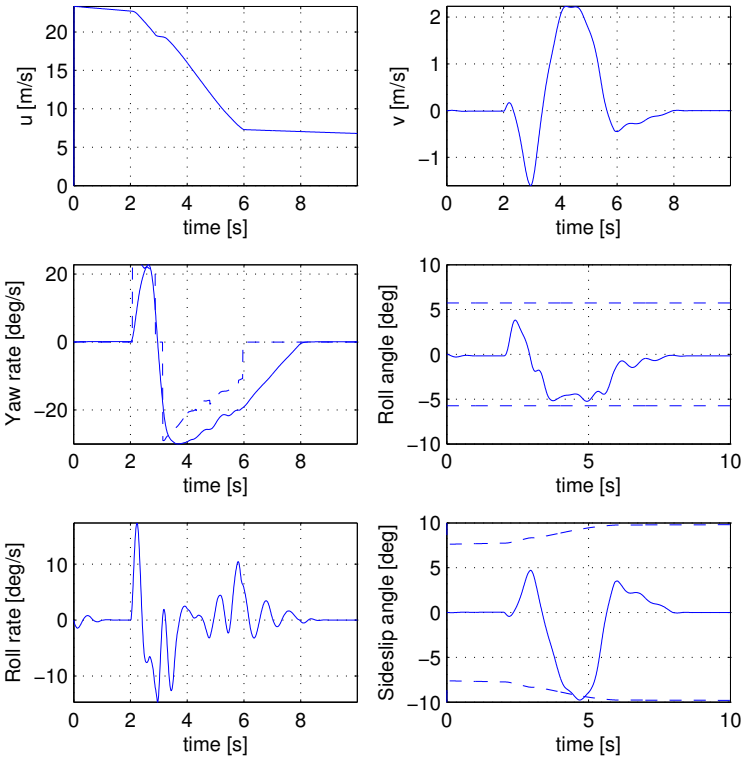

Figure 6.4 Vehicle states during the fishhook maneuver with the controller active. The dashed lines are the yaw rate reference, maximum allowed roll angle and maximum sideslip angle respectively.

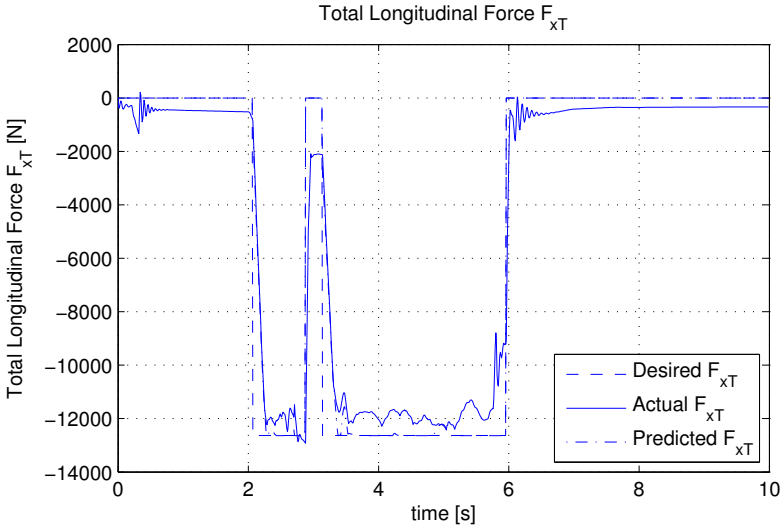

Figure 6.5 Total longitudinal force F_{xT} during the fishhook maneuver.

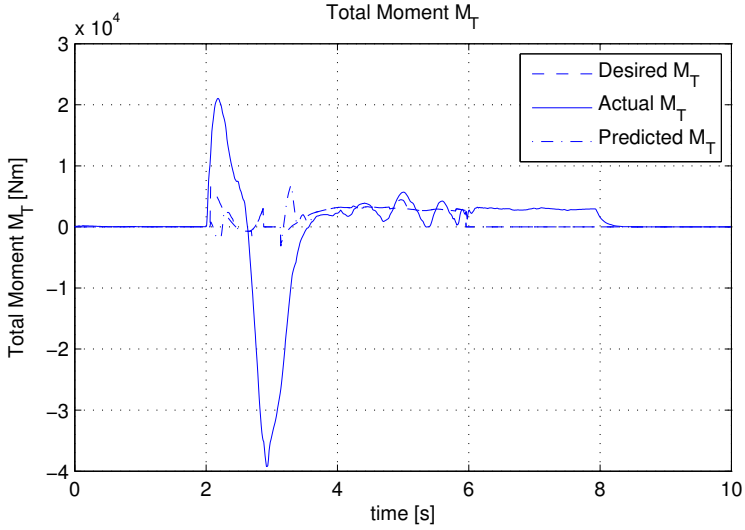

Figure 6.6 Total moment M_T during the fishhook maneuver.

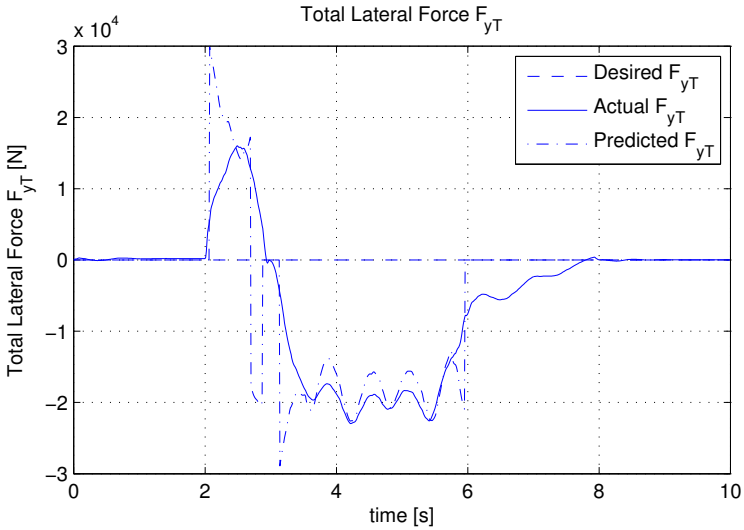

Figure 6.7 Total lateral force F_{yT} during the fishhook maneuver. The total lateral force is not used as a virtual control signal in this strategy. The virtual control command is set to zero, and the corresponding weight in the control allocator is chosen to be small. It is however interesting to observe that the predicted value of F_{yT} calculated by the control allocation algorithm (dotted line) corresponds well with the actual force (solid line).

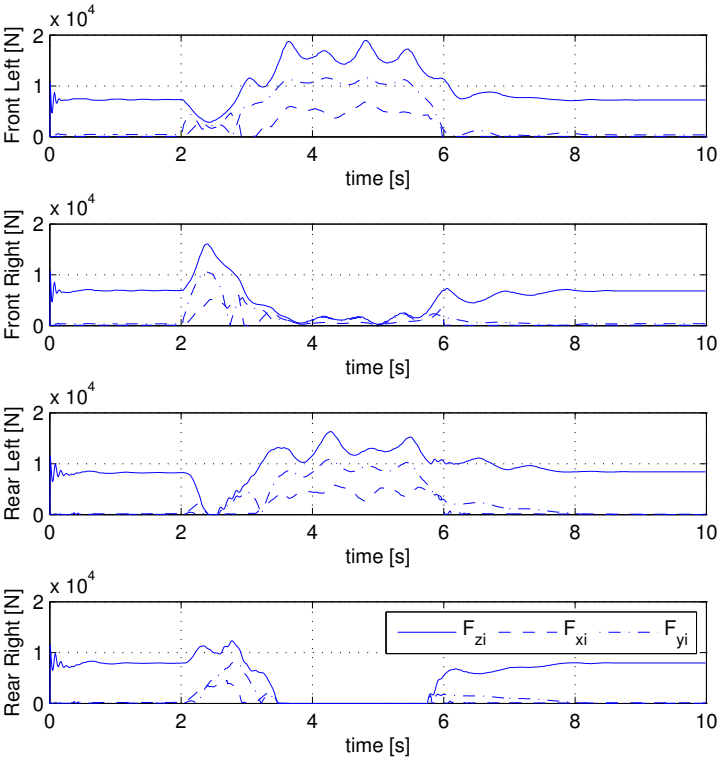

Figure 6.8 Tire forces during the fishhook maneuver with the controller active. The solid lines are the normal forces F_{zi} which, scaled with the friction coefficient μ, correspond to the maximum available force.

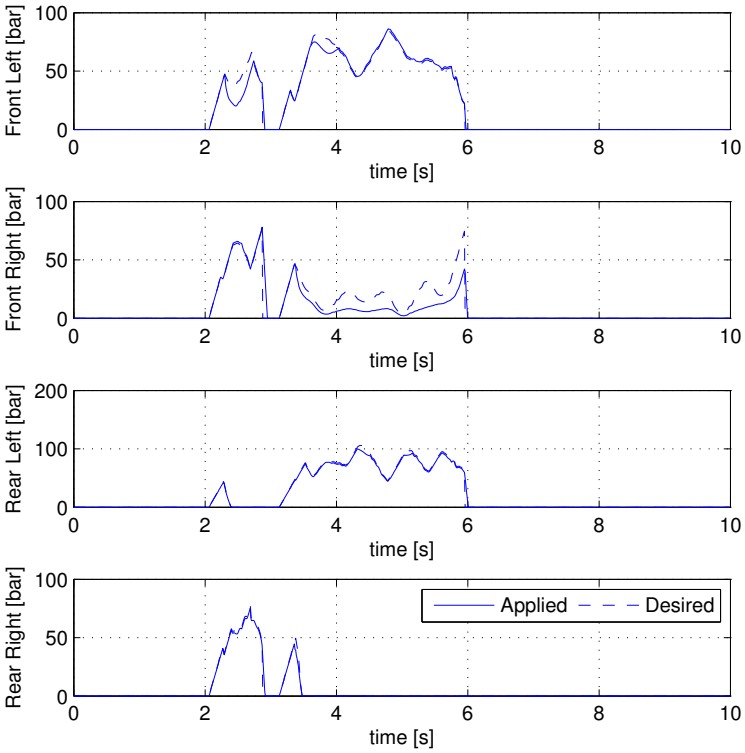

Figure 6.9 The brake pressures for each wheel during the fishhook maneuver. The dotted line is the commanded brake pressure, and the solid line is the achieved brake pressure.

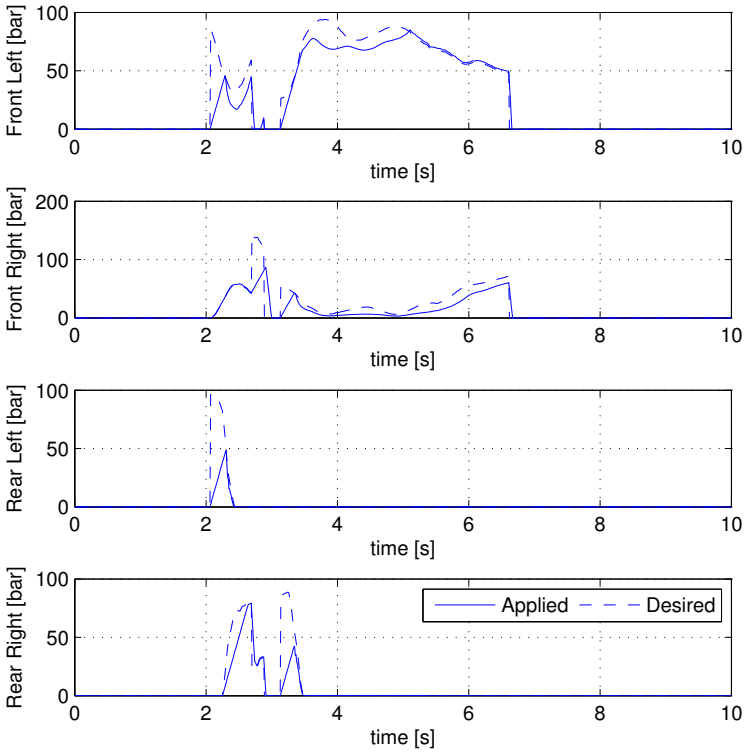

Figure 6.10 The brake pressures for each wheel during the fishhook maneuver, without rate constraints in the control allocator. The discrepancies between the commanded and achieved pressures are clearly seen.

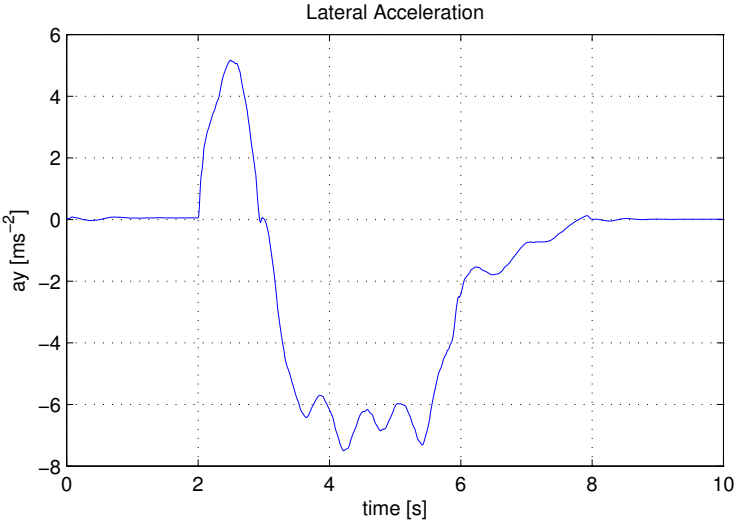

Figure 6.11 The lateral acceleration a_y.

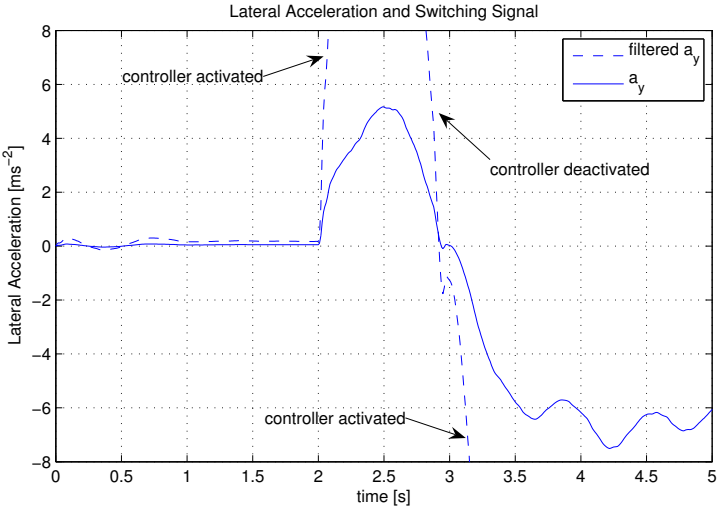

Figure 6.12 A close-up of the lateral acceleration a_y and switching signal $\hat{a}_y$.

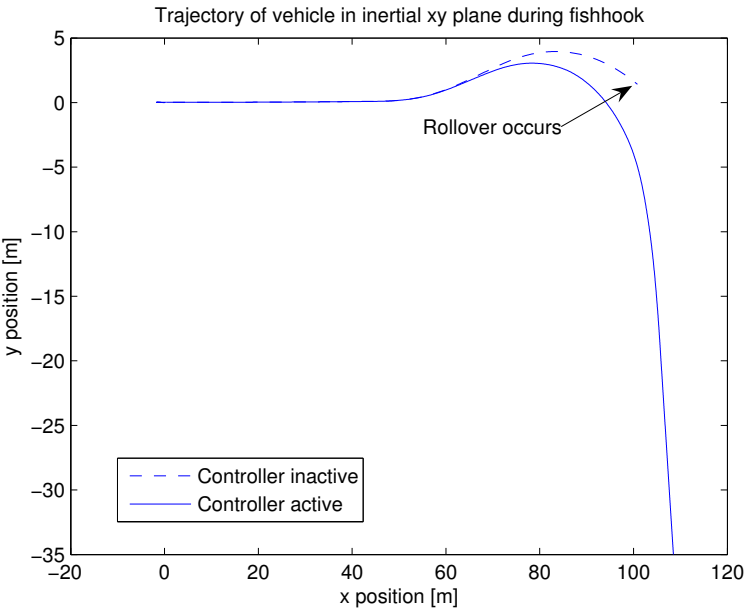

Figure 6.13 Vehicle trajectory in the inertial xy plane during the J-turn maneuver. The solid line corresponds to the trajectory of the vehicle when the controller is active.

Symbol	Description	Value	Unit
m_e	Vehicle mass (empty)	2800	kg
h_e	CG height (empty)	0.79	m
m_b	Load mass	420	kg
h_b	Load height	1	m
h_b	Load distance from front axle	4.2	m
I_{xx}	MI about x–axis	2275	kgm^2
I_{yy}	MI about y–axis	13400	kgm^2
I_{zz}	MI about z–axis (with load)	16088	kgm^2
a	CG distance from front axle	1.58	m
b	CG distance from rear axle	1.97	m
l	Half track width	0.8126	m
C_ϕ	Roll stiffness	221060	Nm/rad
K_ϕ	Roll damping	12160	Nms/rad
μ	Friction coefficient	1	n/a

Table 6.1 Vehicle parameters used in the simulations

J-Turn Maneuver

The control algorithm was tuned using the fishhook maneuver. To test the resulting algorithm, the J-turn maneuver was used. The vehicle states for the J-turn maneuver with the nominal load of 420kg with the controller inactive are shown in Figure 6.14. With the given loading conditions, rollover does not occur, but yaw instability occurs, resulting in a skid (as can be seen from the sideslip angle plot). The vehicle states for the same maneuver with the controller active are shown in Figure 6.15. Both the roll angle and the sideslip angle remain within the desired limits.

This result shows that the proposed VDC system is successful not only in preventing rollover, but also in stabilizing the yaw dynamics for maneuvers in which yaw instability arises without rollover.

Symbol	Description	Value
K_r	Yaw rate controller gain	1
a_x^d	Desired longitudinal deceleration	$0.4g$
$\hat{a}_x^{\text{on}}$	Threshold for controller switching	7
$\hat{a}_x^{\text{off}}$	Threshold for controller switching	5
σ	Tuning parameter in (5.12)	1
ν	Tuning parameter in (5.12)	1
W_v	Weighting matrix in (5.23)	$[1 \quad 100 \quad 30]$
W_u	Weighting matrix in (5.23)	$[1 \quad 1 \quad 1 \quad 1]$
γ	Parameter in (5.23)	10^6

Table 6.2 Controller parameters used in the simulations

Trajectory following Figure 6.16 shows the trajectory of the vehicle during the J-turn maneuver, with and without control. When the controller is active, the vehicle is able to perform a turn with a smaller radius of curvature than the uncontrolled vehicle, which skids. This could be critical in cases when extreme maneuvering is required for collision avoidance.

Robustness In order to test the robustness of the system to uncertainty n the loading conditions, simulations were made using a larger load of 860kg located at a height of 1.3m over the roll axis. The load parameters in the controller were left unchanged. The additional mass and greater height of the load increases the propensity for rollover. Figure 6.17 shows the states of the vehicle with the new loading conditions during a J-turn without control. The greater load causes a rollover to occur. The effects of using the controller (without the correct load parameters) can be seen in Figure 6.18. The controller is capable of preventing rollover, and the yaw dynamics are stabilized. The roll angle is maintained within the desired limits, although the sideslip angle exceeds its limits for a time.

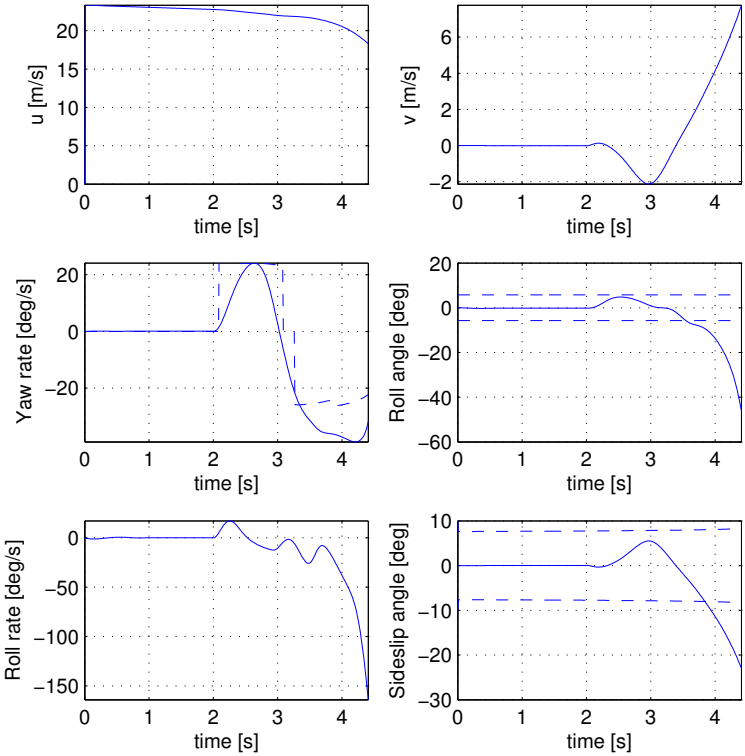

Figure 6.14 Vehicle states for the J-turn maneuver with the controller inactive. The instability of the yaw dynamics and of the sideslip angle is clearly seen.

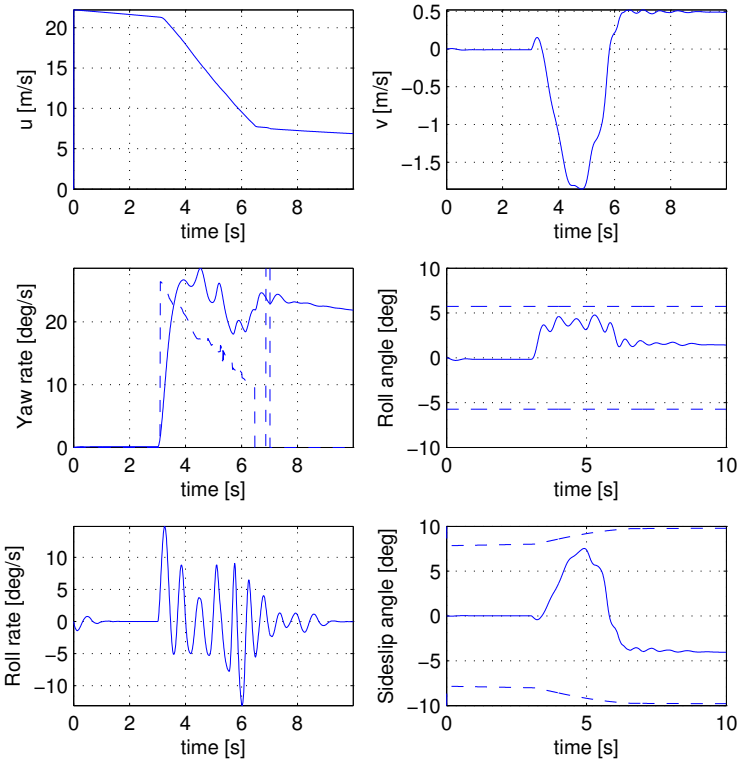

Figure 6.15 Vehicle states for the J-turn maneuver with the controller active. Both the roll angle and the sideslip angle remain within the prescribed limits.

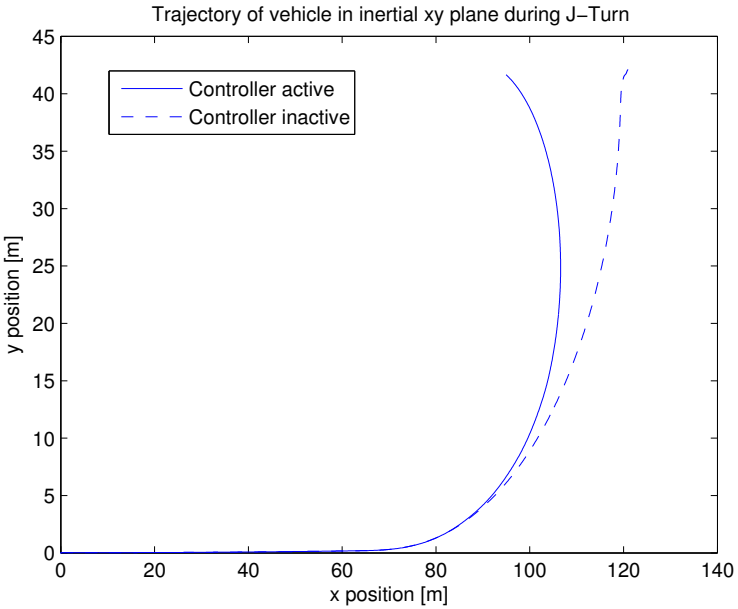

Figure 6.16 Vehicle trajectory in the inertial xy plane during the J-turn maneuver. The solid line corresponds to the trajectory of the vehicle when the controller is active. The controller succeeds in reducing the radius of curvature obtained by the maneuver, as well as stabilizing the yaw dynamics and sideslip angle. This could be extremely important, in the cases when the maneuver is performed in order to avoid an obstacle.

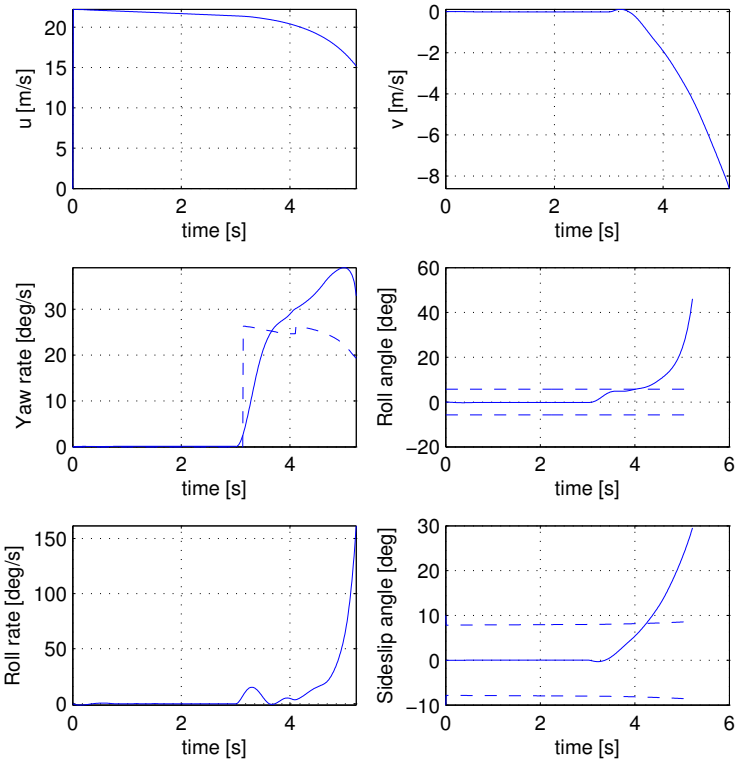

Figure 6.17 Vehicle states for the J-turn maneuver with additional load with the controller inactive. Rollover occurs in this case due to the presence of the additional load.

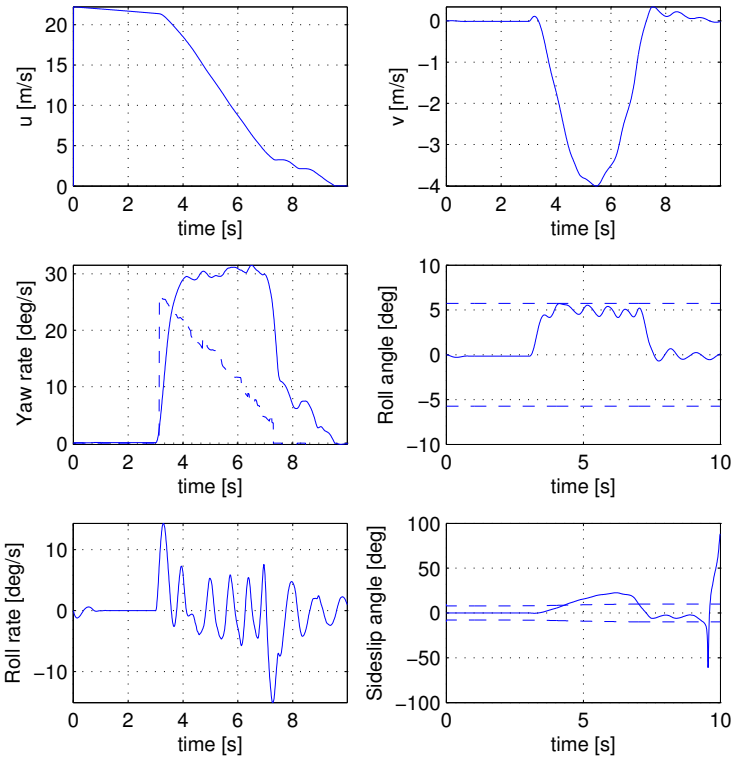

Figure 6.18 Vehicle states for the J-turn maneuver with additional load with the controller active. Rollover is prevented, and the roll angle remains within the prescribed limits. The sideslip angle is stabilized, although it does not remain within the given limits. The behaviour of the sideslip angle in the final second of the simulation is caused by the vehicle coming to rest, and thus may be ignored.

6.4 Discussion

The simulation results presented in this chapter indicate that the proposed algorithms perform well in a number of situations. In this section the peculiarities, merits and drawbacks of the proposed algorithms are discussed.

Rollover Detection and Switching

The proposed PD-based switching method using the lateral acceleration measurement was found to work well. The early detection of an oncoming rollover event is vital to the performance of the overall control system. It was observed that even very small delays in the activation of the controller lead to degraded performance. In particular, the desired values of both the braking force F_{xT} and the total moment M_T can not be met simultaneously. The explanation for this can be found by considering Figure 3.9. As the roll angle, and thus the load transfer, increases, the forces that may be generated by the tires on the inside of the turn decrease. This limits the range of values that may be obtained simultaneously for F_{xT} and M_T. The control allocator attempts to minimize the allocation error for these virtual controls, according to their respective weights, but if the load transfer becomes too large it may be impossible to achieve both desired values at the same time.

Control Strategy

The strategy based on using a threshold value of the lateral acceleration for switching and a P controller for the total braking force, as described in (4.7), is presented in [Schofield *et al.*, 2006]. It was successful in preventing rollover, although oscillations were observed in the control signal. The modified strategy in (4.9) using a constant braking command coupled with the PD detection scheme exhibited better performance. It is conceivable that a more advanced control methodology could be applied to the problem in order to increase the performance. However, more complex strategies are likely to be more dependent on models, and therefore vehicle parameters. Since a reliable scheme for obtaining the necessary parameters has not yet been developed, the design of more complex strategies may be unnecessary.

The yaw rate controller is rather more complex that the roll controller. In simulations it has performed very consistently, the main

problem being the coupling with the total longitudinal force F_{xT}. The desired value of F_{xT} is used for decoupling, which implies that the yaw controller may work poorly in cases when the allocation error is large, that is, when the desired virtual controls cannot be achieved.

Control Allocation

Tire Force Approximation The proposed control allocation strategy, based on the use of linear approximations of the tire force characteristics, worked remarkably well. The approximation, given by:

$$\nu F_y = (\sigma \mu F_z + F_x)\text{sign}(\delta)$$

originates from the assumption that tire forces are permanently saturated when the controller is active. This implies that the maximum achievable lateral forces depend only on the friction coefficient and the normal force, and not on the slip angles. This is useful since the slip angles are not measurable. Although this constitutes a major assumption, it was found that this assumption appeared to be valid. Figures 6.5, 6.6 and 6.7 show that the values of F_{xT}, F_{yT} and M_T that were obtained closely match the values predicted by the model used in the control allocator. In fact, the tuning parameters ν and σ were not required; the algorithm worked very well with both parameters set to one. This is of course related to the fact that the friction coefficient was assumed to be known.

Warmstarting The use of the optimal point and active set from the previous sample time as a starting point for the next sample time was found to be very useful in reducing the computation time necessary for obtaining the solution of the control allocation problem. A C-code implementation of the weighted least squares control allocation strategy from the QCAT toolbox was used in the simulations. Information about the computation times required for computing the solution of the control allocation problem is shown in Table 6.3. The data relates to a fishhook maneuver, and the simulation was performed on a computer with a 1.83GHz Core Duo processor and 1Gb RAM.

The mean execution time is two orders of magnitude smaller than the sampling time of 10ms, and the maximum execution time is one

Mean execution time	0.1965 ms
Maximum execution time	0.8976 ms
Standard deviation	0.1805 ms

Table 6.3 Execution time data for the control allocation solver. The data relates to a fishhook maneuver.

order of magnitude smaller. Although a powerful computer was used in the simulations, it is clear that real-time performance can be obtained with reasonable hardware.

Summary

In this chapter simulation results have been presented which confirm the operation of the proposed vehicle dynamics control algorithm. Standard test maneuvers relevant for rollover prevention have been used as test cases. Although simulation by itself cannot conclusively demonstrate the effectiveness of the algorithms, the advanced nature of the simulator used ensures a high level of realism, and negates many issues such as unmodeled dynamics. Nevertheless, it is important to be conscious of the fact that problems such as parameter uncertainties may present themselves in real-world experiments.

7

Conclusions and Future Work

7.1 Summary

In this thesis a control strategy for a vehicle dynamics control system has been presented. The primary aim of the system is the prevention of vehicle rollover, but the system also has similar functionality to today's Electronic Stability Program (ESP) systems in terms of yaw control. This follows the current trend in automotive control design towards the integration of control systems.

The control strategy is based on the use of control allocation, where the control design is performed with respect to generalized forces or virtual controls, which are then mapped to actuator commands. This mapping is nontrivial, since a number of constraints must be taken into account. The control allocation strategy uses convex optimization to obtain an optimal mapping from virtual controls to actuator commands, guaranteeing that the constraints are not violated. The use of convex optimization in this context requires careful formulation of the problem in order to obtain an algorithm suitable for real-time implementation.

7.2 Conclusions

The strategy has been shown to work well in simulations with a highly realistic vehicle model. The algorithm was observed to be capable of robustly preventing rollover, and relatively little tuning was required to obtain good performance.

Control Allocation

The linear tire force approximation, which was important for the formulation of a suitable quadratic programming problem in the control allocation strategy, was shown to be valid. The resulting QP problem can be solved fast enough to allow real-time implementation, and the control allocator was shown to be capable of accurately reproducing the desired generalized forces.

The strategy has a number of advantages over existing methods, which typically use rule-based algorithms to determine how braking force should be distributed. All of the wheels are used as actuators, rather than only the front wheels. The tuning parameters are few in number and are intuitive to understand. It was observed that relatively little tuning of the control allocator was required in order to achieve good performance.

7.3 Future Work

Vehicle trials

Although the algorithm performs well in simulations, experiments are required in order to confirm the operation of the algorithm in a real vehicle. It is intended to test the algorithm in an actual vehicle within the near future. It is expected that issues such as knowledge of vehicle parameters, the coefficient of friction, and the quality state estimation will be important factors in the experiments.

Adaptation

The current algorithm assumes knowledge of a number of important parameters, such as the friction coefficient and loading conditions. Although information is sometimes available about these parameters, it

is likely that performance could be improved through the use of adaptation. For example, the tuning parameters in the linear tire force approximation used in the control allocator could be obtained using some form of direct adaptive scheme based on a performance criterion. Additionally, the loading conditions could be estimated online. Such a strategy would most likely run continuously, independent of the controller. A common problem with adaptation in automotive applications is the issue of persistency of excitation, which cannot be guaranteed.

Robustness

As previously stated, the strategy has been observed to be robust in the simulations, in the sense that rollover is prevented for a wide range of parameter values and operating conditions. However, it is concievable that more could be done in the control design to guarantee robustness. The use of nonlinear damping to counteract the effects of uncertainty in the yaw rate control design is an example of this.

Control Allocation

Since control allocation is most often based on the formulation of optimization problems, there are many different options available. Examples of other methods that could be used include multiparametric nonlinear programming [Tøndel and Johansen, 2005], as well as adaptive dynamic control allocation [Tjønnås and Johansen, 2005].

8

Bibliography

Bengtsson, J. (2004): *Closed-Loop Control of HCCI Engine Dynamics*. PhD thesis ISRN LUTFD2/TFRT--1070--SE, Department of Automatic Control, Lund Institute of Technology, Lund University, Sweden.

Boyd, S. and L. Vandenberghe (2004): *Convex Optimization*. Cambridge University Press, New York, NY, USA.

Carlson, C. R. and J. C. Gerdes (2003): "Optimal rollover prevention with steer by wire and differential braking." In *Proceedings of the ASME International Mechanical Engineering Congress and Exposition*. Washington, D.C. USA.

Chen, B. and H. Peng (2001): "Differential-braking-based rollover prevention for sport utility vehicles with human-in-the-loop evaluations." *Vehicle System Dynamics*, **36:4–5**, pp. 359–389.

Chen, B. C. and H. Peng (1999): "A real-time rollover threat index for sports utility vehicles." In *Proceedings of the American Control Conference*.

Chen, B. C. and H. Peng (2000): "Rollover prevention for sports utility vehicles with human-in-the-loop evaluations." In *5th Int'l Symposium on Advanced Vehicle Control*.

Dahlberg, E. (2001): *Commercial Vehicle Stability - Focusing on Rollover*. PhD thesis, Royal Institute of Technology, Stockholm, Sweden.

Forkenbrock, G. J., W. Garrot, M. Heitz, and B. C. O'Harra (2002): "A comprehensive experimental examination of test maneuvers that may induce on-road, untripped, light vehicle rollover - phase iv of nhtsa's light vehicle rollover research program." Technical Report. National Highway Traffic Safety Administration.

Gäfvert, M. (2003): *Topics in Modeling, Control, and Implementation in Automotive Systems*. PhD thesis ISRN LUTFD2/TFRT--1066--SE, Department of Automatic Control, Lund Institute of Technology, Sweden.

Gillespie, T. N. (1992): *Fundamentals of Vehicle Dynamics*. Society of Automotive Engineers, Warrendale, PA.

Härkegård, O. (2003): *Backstepping and Control Allocation with Applications to Flight Control*. PhD thesis Linköping Studies in Science and Technology. Thesis No 820, Department of Electrical Engineering, Linköping University, SE–581 83 Linköping, Sweden.

Imsland, L., T. A. Johansen, T. I. Fossen, J. C. Kalkkuhl, and A. Suissa (2005): "Vehicle velocity estimation using modular nonlinear observers." In *IEEE Conf. Decision and Control, Sevilla, Spain*.

Jansson, J. (2005): *Collision Avoidance Theory with Application to Automotive Collision Mitigation*. PhD thesis Linköping Studies in Science and Technology. Dissertations. No. 950, Linköping University, Linköping University, 581 83 Linköping, Sweden.

Johansson, B. and M. Gäfvert (2004): "Untripped suv rollover detection and prevention." In *43rd IEEE Conference on Decision and Control*.

Johansson, R. and A. Rantzer, Eds. (2003): *Nonlinear and Hybrid Systems in Automotive Control*. Springer-Verlag, London. ISBN 1-85233-652-8.

Khalil, H. (2002): *Nonlinear Systems*, third edition. Prentice Hall.

Kiencke, U. and L. Nielsen (2000): *Automotive Control Systems: For Engine, Driveline and Vehicle*. Springer-Verlag New York, Inc., Secaucus, NJ, USA.

Kristić, M., I. Kanellakoopulos, and P. Kokotović (1995): *Nonlinear and Adaptive Control Design*. John Wiley & Sons.

Mitschke, M. (1995): *Dynamik der Kraftfahrzeuge*, third edition. Springer.

Odenthal, D., T. Bunte, and J. Ackermann (1999): "Nonlinear steering and braking control for vehicle rollover avoidance."

Pacejka, H. B. (2002): *Tyre and Vehice Dynamics*. Butterworth Heinemann.

Plumlee, J. H., D. M. Bevley, and A. S. Hodel (2004): "Control of a ground vehicle using quadratic programming based control allocation techniques." In *Proceedings of the American Control Conference*. Boston, Massachusetts, USA.

Schofield, B., T. Hägglund, and A. Rantzer (2006): "Vehicle dynamics control and controller allocation for rollover prevention." In *Proceedings of the IEEE International Conference on Control Applications*. Munich, Germany.

Slotine, J. E. and W. Li (1991): *Applied Nonlinear Control*. Prentice Hall.

Solyom, S. (2004): *Control of Systems with Limited Capacity*. PhD thesis ISRN LUTFD2/TFRT--1069--SE, Department of Automatic Control, Lund Institute of Technology, Sweden.

Spiegel, M. R. (1967): *Theory and Problems of Theoretical Mechanics*. Schaum Publishing.

Svendenius, J. (2003): "Tire models for use in braking applications." Licentiate Thesis ISRN LUTFD2/TFRT--3232--SE. Department of Automatic Control, Lund University, Sweden.

Tjønnås, J. and T. A. Johansen (2005): "Optimizing nonlinear adaptive control allocation." In *IFAC World Congress*. Prague, Czech Republic.

Tøndel, P. and T. A. Johansen (2005): "Control allocation for yaw stabilization in automotive vehicles using multiparametric nonlinear programming." In *American Control Conference*.

Wong, J. Y. (1993): *Theory of Ground Vehicles*, second edition. John Wiley and Sons.

Department of Automatic Control
Lund University
Box 118
SE-221 00 Lund Sweden

Document name
LICENTIATE THESIS

Date of issue

Document Number
ISRN LUTFD2/TFRT--3241--SE

Author(s)
Brad Schofield

Supervisor
Tore Hägglund
Anders Rantzer

Sponsoring organisation
EU 6th Framework Project CEmACS

Title and subtitle
Vehicle Dynamics Control for Rollover Prevention

Abstract

Vehicle rollover accidents are a particularly dangerous form of road accident. Existing vehicle dynamics controllers primarily deal with yaw stability, and are of limited use for dealing with problems of roll instability. This thesis deals with the development of a new type of vehicle dynamics control system, capable of preventing rollover accidents caused by extreme maneuvering.

A control strategy based on limitation of the roll angle while following a yaw rate reference is presented. Methods for rollover detection are investigated. A new computationally–efficient control allocation strategy based on convex optimization is used to map the controller commands to the individual braking forces, taking into account actuator constraints. Simulations show that the strategy is capable of preventing rollover of a commercial van during various standard test maneuvers.

Key words
Vehicle Dynamics, Rollover Prevention, Control Allocation, Convex Optimization, Nonlinear Control

Classification system and/or index terms (if any)

Supplementary bibliographical information

ISSN and key title
0280–5316

ISBN

Language
English

Number of pages
108

Recipient's notes

Security classification